# Calcium influx promotes PLEKHG4B localization to cell–cell junctions and regulates the integrity of junctional actin filaments

Komaki Ninomiya[a,b], Kai Ohta[a], Ukyo Kawasaki[a], Shuhei Chiba[a], Takanari Inoue[c], Erina Kuranaga[b,d], Kazumasa Ohashi[a,e,*], and Kensaku Mizuno[a,e,*]

[a]Laboratory of Molecular and Cellular Biology, and [b]Laboratory for Histogenetic Dynamics, Graduate School of Life Sciences, Tohoku University, Aobayama, Sendai, Miyagi 980-8578, Japan; [c]Department of Cell Biology and Center for Cell Dynamics, Johns Hopkins University School of Medicine, Baltimore, MD 21205; [d]Laboratory for Histogenetic Dynamics, Graduate School and Faculty of Pharmaceutical Sciences, Kyoto University, Kyoto 606-8304, Japan; [e]Department of Chemistry, Graduate School of Science, Tohoku University, Aobayama, Sendai, Miyagi 980-8578, Japan

**ABSTRACT** **PLEKHG4B is a Cdc42-targeting guanine-nucleotide exchange factor implicated in forming epithelial cell–cell junctions. Here we explored the mechanism regulating PLEKHG4B localization. PLEKHG4B localized to the basal membrane in normal $Ca^{2+}$ medium but accumulated at cell–cell junctions upon ionomycin treatment. Ionomycin-induced junctional localization of PLEKHG4B was suppressed upon disrupting its annexin-A2 (ANXA2)-binding ability. Thus, $Ca^{2+}$ influx and ANXA2 binding are crucial for PLEKHG4B localization to cell–cell junctions. Treatments with low $Ca^{2+}$ or BAPTA-AM (an intracellular $Ca^{2+}$ chelator) suppressed PLEKHG4B localization to the basal membrane. Mutations of the phosphoinositide-binding motif in the pleckstrin homology (PH) domain of PLEKHG4B or masking of membrane phosphatidylinositol-4,5-biphosphate [$PI(4,5)P_2$] suppressed PLEKHG4B localization to the basal membrane, indicating that basal membrane localization of PLEKHG4B requires suitable intracellular $Ca^{2+}$ levels and $PI(4,5)P_2$ binding of the PH domain. Activation of mechanosensitive ion channels (MSCs) promoted PLEKHG4B localization to cell–cell junctions, and their inhibition suppressed it. Moreover, similar to the PLEKHG4B knockdown phenotypes, inhibition of MSCs or treatment with BAPTA-AM disturbed the integrity of actin filaments at cell–cell junctions. Taken together, our results suggest that $Ca^{2+}$ influx plays crucial roles in PLEKHG4B localization to cell–cell junctions and the integrity of junctional actin organization, with MSCs contributing to this process.**

## SIGNIFICANCE STATEMENT

- PLEKHG4B, a Cdc42-targeting GEF, is localized to cell–cell junctions and implicated in cell–cell junction organization. The mechanism underlying junctional localization of PLEKHG4B is not known.
- The authors showed that ionomycin- or mechanosensitive channel (MSC)-mediated $Ca^{2+}$ influx promotes PLEKHG4B localization to cell–cell junctions, with the help of annexin-A2 and phosphatidylinositol-4,5-bisphosphate. PLEKHG4B knockdown and inhibition of MSCs similarly impaired actin organization at cell–cell junctions, suggesting that MSC-mediated $Ca^{2+}$ influx and subsequent PLEKHG4B localization to cell–cell junctions play a crucial role in the integrity of cell–cell junctions.
- These findings provide insights into how mechanical forces regulate cell–cell adhesions.

**Monitoring Editor**
Alpha Yap
University of Queensland

Received: May 3, 2023
Revised: Nov 1, 2023
Accepted: Dec 7, 2023

This article was published online ahead of print in MBoC in Press (http://www.molbiolcell.org/cgi/doi/10.1091/mbc.E23-05-0154) on December 13, 2023.

*Address correspondence to: Kazumasa Ohashi (kazumasa.ohashi.b2@tohoku.ac.jp); Kensaku Mizuno (kensaku.mizuno.d8@tohoku.ac.jp).

Abbreviations used: AMPK, AMP-activated protein kinase; ANXA2, annexin-A2; CAMKK2, $Ca^{2+}$/calmodulin-dependent kinase kinase 2; CFP, cyan fluorescent protein; DH, Dbl homology; DMSO, dimethyl sulfoxide; FKBP, FK506-binding protein; FL, full-length; FRB, FKBP-rapamycin binding; GEF, guanine nucleotide exchange factor; GFP, green fluorescent protein; MDCK, Madin-Darby canine kidney; MoA, monoamine oxidase A; MSC, mechanosensitive ion channel; PH, pleckstrin homology; PH(PLCδ), PH domain of phospholipase C-δ1; PI(4)P, phosphatidylinositol-4-phosphate; PI(4)P5K, PI(4)P 5-kinase; $PI(4,5)P_2$, phosphatidylinositol-4,5-bisphosphate; PLEKHG4B, pleckstrin homology domain-containing family G member 4B; siRNA, small interfering RNA; WT, wild-type; YFP, yellow fluorescent protein.

## INTRODUCTION

Cell–cell junctions play fundamental roles in the formation, remodeling, and function of epithelial tissues by regulating various epithelial cell properties, including morphology, polarity, motility, proliferation, mechanical integrity, and barrier function (Garcia *et al.*, 2018). Defects in epithelial cell–cell junctions are associated with various diseases, including cardiovascular diseases and cancer. Epithelial cells adhere to each other through separate junctional complexes, typically comprising tight junctions, adherens junctions, and desmosomes. Of these, adherens junctions interconnect adjacent cells through the homophilic association of cadherins, a family of calcium-dependent transmembrane cell–cell adhesion proteins. The cytoplasmic regions of cadherins are linked to actin filaments via adherens junction-associated proteins, such as α- and β-catenin (Harris and Tepass, 2010; Takeichi, 2014; Mège and Ishiyama, 2017). While actin cytoskeletal organization is controlled by cadherin-mediated cell–cell adhesions, the formation and remodeling of cell–cell adhesions are regulated by actin cytoskeletal dynamics and actomyosin-based contractility (Takeichi, 2014; Lecuit and Yap, 2015). Notably, cells in epithelial tissues are continuously exposed to mechanical forces at cell–cell junctions, implying that mechanical force-induced actin remodeling plays a crucial role in the dynamics and remodeling of cell–cell junctions (Takeichi, 2014; Lecuit and Yap, 2015; Ohashi *et al.*, 2017; Varadarajan *et al.*, 2022).

Rho family small GTPases, such as RhoA, Rac1, and Cdc42, play a key role in actin cytoskeletal reorganization (Hodge and Ridley, 2016). They are activated by Rho-guanine nucleotide exchange factors (Rho-GEFs), which stimulate Rho GTPase conversion from inactive GDP-bound forms to active GTP-bound forms; these activated forms associate with downstream effector proteins and thereby induce actin cytoskeletal remodeling (Hodge and Ridley, 2016). The human genome encodes ~70 members of the Dbl-like Rho-GEF gene family (Rossman *et al.*, 2005; Cook *et al.*, 2014). These proteins commonly possess two functional domains, a Dbl homology (DH) domain responsible for their GEF catalytic activity, and a pleckstrin homology (PH) domain, which mediates membrane association of Rho-GEFs or modulates the GEF activity of the DH domain (Cook *et al.*, 2014). Previous studies have shown that Rho-GEFs and Rho GTPases are involved in the formation and remodeling of cell–cell junctions by regulating actin cytoskeletal reorganization; inversely, cadherin-based cell–cell adhesions control the activities of Rho GTPases (Fukata and Kaibuchi, 2001; McCormack *et al.*, 2013; Citi *et al.*, 2014; Arnold *et al.*, 2017; Braga, 2018). Thus, Rho GTPases and cadherins mutually regulate their activities during the formation and remodeling of cell–cell adhesions. However, the precise mechanisms underlying actin cytoskeletal organization during the formation and remodeling of cell–cell adhesions and the roles of Rho-GEFs in these processes remain unclear (McCormack *et al.*, 2013; Takeichi, 2014).

We recently showed that PH domain-containing family G member 4B (PLEKHG4B), a member of the Dbl-like Rho-GEF family that principally targets Cdc42, is involved in actin cytoskeletal remodeling during epithelial cell–cell junction formation (Ninomiya *et al.*, 2021). Knockdown of PLEKHG4B impairs the formation of "closed junctions" with closely packed actin bundles along the cell–cell contacts. PLEKHG4B localizes to the basal membrane and cell–cell junctions and binds to annexin A2 (ANXA2). Knockdown of ANXA2 suppresses junctional localization of PLEKHG4B, indicating that ANXA2 is involved in PLEKHG4B localization to cell–cell junctions (Ninomiya *et al.*, 2021). ANXA2 is a $Ca^{2+}$- and phosphoinositide-binding protein that mediates plasma membrane localization of various proteins and regulates actin dynamics at specific membrane sites (Gerke *et al.*, 2005; Bharadwaj *et al.*, 2013). Thus, intracellular calcium signals and membrane phosphoinositides might be involved in the localization of PLEKHG4B. However, their roles in PLEKHG4B localization remain to be explored.

Calcium signaling plays pivotal roles in transducing various chemical and mechanical cues into diverse cell responses, including actin cytoskeletal remodeling and cell–cell junction formation (Clapham, 2007; Tsai *et al.*, 2015). E-cadherin requires extracellular calcium ions for its homophilic association to establish cell–cell adhesions between adjacent cells; intracellular calcium signals are also implicated in regulating the activity of Rho family GTPases and actin cytoskeletal reorganization (Benink and Bement, 2005; Clark *et al.*, 2009; Murakoshi *et al.*, 2011; Pardo-Pastor *et al.*, 2018), suggesting the important role of calcium signaling in the formation and remodeling of cell–cell adhesions. Recent studies have shown that mechanosensitive ion channel (MSC)-mediated calcium influx regulates actin cytoskeleton during cell–cell junction remodeling (Rajakylä *et al.*, 2020; Varadarajan *et al.*, 2022) and filopodial protrusions through Cdc42 activation (Yang *et al.*, 2020). However, the mechanism underlying intracellular $Ca^{2+}$ signal-mediated cell–cell adhesion remodeling is largely unknown.

In this study, we investigate the role of calcium and phosphoinositide signals in PLEKHG4B localization. We demonstrate that PLEKHG4B localizes to the basal membrane in normal $Ca^{2+}$ medium but accumulates at cell–cell junctions after ionomycin treatment. We provide evidence that $Ca^{2+}$ influx and ANXA2 binding are crucial for ionomycin-induced PLEKHG4B localization to the cell–cell junctions and that appropriate levels of intracellular $Ca^{2+}$ and phosphoinositide-binding ability of the PH domain are required for PLEKHG4B localization to the basal membrane in normal $Ca^{2+}$ medium. We also provide evidence that MSCs-mediated $Ca^{2+}$ influx plays crucial roles in PLEKHG4B localization to the basal membrane and cell–cell junctions and the integrity of actin organization at cell–cell junctions.

## RESULTS

### Calcium ionophore induces PLEKHG4B localization to cell–cell junctions

PLEKHG4B preferentially localizes to the basal membrane and cell–cell junctions in epithelial cells and plays a crucial role in forming cell–cell adhesions (Ninomiya *et al.*, 2021). To explore the mechanism regulating the subcellular localization of PLEKHG4B, we examined the effect of calcium influx on PLEKHG4B localization by treating Madin-Darby canine kidney (MDCK) epithelial cells with a calcium ionophore, ionomycin. Time-lapse fluorescence analyses using a $Ca^{2+}$ indicator GCaMP6 (Ohkura *et al.*, 2012) showed that treatment of MDCK cells with 2.5 μM ionomycin caused rapid elevation of intracellular $Ca^{2+}$ and the high level of $Ca^{2+}$ was maintained at least 15 min after the treatment with ionomycin (Supplemental Figure S1A). MDCK cells were transfected with yellow fluorescent protein (YFP)-tagged PLEKHG4B or control YFP, cultured for 24 h to reach a subconfluent state, and then treated with ionomycin or vehicle (DMSO) for 15 min. Cells were then stained with rhodamine-labeled phalloidin for visualizing actin filaments and immunostained with an anti-α-catenin antibody for visualizing adherens junctions. Confocal microscopic analyses at the basal, medial, and apical planes revealed that YFP-PLEKHG4B predominantly localized to the central region of the basal membrane in vehicle-treated cells and was translocated to cell–cell junctions in the basal plane after ionomycin treatment (Figure 1A). In contrast, control YFP was diffusely distributed throughout the cell in both vehicle- and ionomycin-treated cells. Live imaging of GFP-PLEKHG4B in MDCK cells also demonstrated that ionomycin

treatment induces PLEKHG4B localization to cell–cell junctions (Supplemental Movie 1). The x-z image analyses clearly showed predominant localization of PLEKHG4B on the basal plane of the cell in vehicle-treated cells and its accumulation at the cell–cell junctions after ionomycin treatment (Figure 1B). Quantitative analyses showed that ionomycin treatment significantly increased the number of cells with junctional localization of PLEKHG4B and the intensity of PLEKHG4B at cell–cell junctions (Figure 1, C and D). Coincident with the changes in PLEKHG4B localization, actin filaments were accumulated at the central region of the basal membrane in vehicle-treated cells and at the cell–cell junctions in ionomycin-treated cells (Figure 1, A and B). These results suggest that ionomycin-induced calcium influx induces PLEKHG4B accumulation at cell–cell junctions and thereby promotes junctional actin filament assembly.

We next examined the time-dependent changes in PLEKHG4B localization after ionomycin treatment in MDCK cell lines stably expressing V5 epitope-tagged PLEKHG4B (MDCK/V5-PLEKHG4B cells). Cells were cultured for 48 h and then treated with ionomycin. At 0, 5, 15, and 30 min after ionomycin treatment, the cells were fixed and stained with rhodamine-phalloidin and with anti-V5 and anti-α-catenin antibodies. Similar to the results of YFP-PLEKHG4B-transfected cells, confocal microscopic analyses of the basal plane revealed that V5-PLEKHG4B localized to the basal membrane at 0 min, and was translocated to cell–cell junctions at 15 and 30 min in MDCK/V5-PLEKHG4B cells (Figure 1E); no V5 signal was detected in parental cells (Supplemental Figure S1B). Quantitative analyses showed that ionomycin treatment for 15 min significantly increased the number of cells with junctional localization of V5-PLEKHG4B and the intensity of V5-PLEKHG4B at cell–cell junctions (Figure 1, F and G). In V5-PLEKHG4B-expressing cells, concomitantly with PLEKHG4B localization, actin filaments were accumulated at the basal membrane at 0 min and at cell–cell junctions at 15–30 min (Figure 1E; Supplemental Figure S1C). Additionally, the α-catenin signals at the cell–cell junctions significantly increased upon ionomycin treatment in both parental and MDCK/V5-PLEKHG4B cells (Figure 1, E and H). These results suggest that PLEKHG4B primarily localizes to the basal membrane in normal $Ca^{2+}$ medium and that ionomycin-induced $Ca^{2+}$ influx promotes its translocation to cell–cell junctions with concomitant accumulation of actin filaments and α-catenin at the cell–cell junctions.

To examine the localization of PLEKHG4B with the expression level similar to that of endogenous protein, we constructed CRISPR/Cas9-mediated knock-in MDCK cells, in which GFP-PLEKHG4B sequence was inserted into the 5′UTR of the PLEKHG4B gene locus (Supplemental Figure S2) and analyzed its localization. GFP-PLEKHG4B localized to the basal membrane in vehicle-treated cells and accumulated at cell–cell junctions after ionomycin treatment (Figure 1I), the phenomena similar to those observed in YFP- or V5-PLEKHG4B-expressing cells.

### Effects of low $Ca^{2+}$ treatment or intracellular $Ca^{2+}$ chelation on PLEKHG4B localization

We next examined the effects of low $Ca^{2+}$ treatment on PLEKHG4B localization. MDCK cells transfected with YFP-PLEKHG4B or YFP were cultured for 48 h in normal $Ca^{2+}$ medium, and then cultured for 3 h in low $Ca^{2+}$ medium. In both YFP- and YFP-PLEKHG4B-expressing cells, low $Ca^{2+}$ treatment decreased the E-cadherin signals at cell–cell junctions and caused disruption of cell–cell contacts (Figure 2A). In YFP-PLEKHG4B-expressing cells, YFP-PLEKHG4B and actin filaments accumulated on the central region of the basal membrane in normal $Ca^{2+}$ medium, but their fluorescent signals at the basal membrane were markedly decreased upon low $Ca^{2+}$ treatment (Figure 2A). These results suggest that normal levels of $Ca^{2+}$ in the culture medium are required for PLEKHG4B localization to the basal membrane.

To examine whether the decreased basal membrane localization of PLEKHG4B in low $Ca^{2+}$ medium is caused by the disruption of E-cadherin-mediated cell–cell adhesions or the deprivation of intracellular $Ca^{2+}$, we analyzed the effect of E-cadherin knockdown on PLEKHG4B localization. MDCK/V5-PLEKHG4B cells were transfected with control or E-cadherin-targeting siRNAs, cultured for 48 h, and then treated with ionomycin for 15 min. Suppression of E-cadherin expression was confirmed by immunoblot analysis (Figure 2B). The α-catenin signals at the cell–cell junctions were decreased in E-cadherin-knockdown cells, indicating that E-cadherin knockdown effectively disrupted cell–cell adhesions (Figure 2C). In cells treated with control siRNA, V5-PLEKHG4B and actin filaments localized to the basal membrane in vehicle-treated cells and accumulated to cell–cell junctions upon ionomycin treatment (Figure 2C), as described above. E-cadherin knockdown had no apparent effect on either the basal membrane localization of PLEKHG4B in vehicle-treated cells or its accumulation to cell–cell junctions in ionomycin-treated cells; thus, E-cadherin-mediated cell–cell adhesion is not principally involved in either the basal membrane localization of PLEKHG4B in normal $Ca^{2+}$ medium or its accumulation to cell–cell junctions after ionomycin treatment. These results indicate that the intracellular $Ca^{2+}$ concentration, rather than the E-cadherin-mediated cell–cell adhesion, primarily contributes to PLEKHG4B localization to the basal membrane in normal $Ca^{2+}$ medium and its accumulation to cell–cell junctions upon ionomycin treatment.

To further examine the role of intracellular $Ca^{2+}$ concentration in PLEKHG4B localization, we analyzed the effect of treatment with BAPTA-AM (a cell-permeable $Ca^{2+}$ chelator) on the localization of PLEKHG4B. MDCK cells expressing YFP-PLEKHG4B were pretreated with BAPTA-AM for 15 min and then treated with ionomycin for 15 min. The cells were then fixed and stained with phalloidin and an anti-β-catenin antibody. Without BAPTA-AM treatment, PLEKHG4B localized to the basal membrane in ionomycin-untreated cells and accumulated at cell–cell junctions upon ionomycin treatment. In contrast, pretreatment with BAPTA-AM suppressed PLEKHG4B localization either to the basal membrane in ionomycin-untreated cells or its accumulation at cell–cell junctions in ionomycin-treated cells, resulting in its diffuse distribution in the cytoplasm (Figure 2D). Live imaging of mCherry-PLEKHG4B in MDCK cells also showed that PLEKHG4B localization to the basal membrane decreased after BAPTA-AM treatment (Supplemental Movie 2). These results further support the view that normal levels of intracellular $Ca^{2+}$ are required for PLEKHG4B localization to the basal membrane and that the $Ca^{2+}$ influx is involved in its accumulation to cell–cell junctions upon ionomycin treatment.

### AnnexinA2 is required for PLEKHG4B localization to cell–cell junctions

ANXA2 is a $Ca^{2+}$- and phosphoinositide-binding protein that mediates membrane localization of various proteins (Gerke *et al.*, 2005). We previously reported that ANXA2 binds to PLEKHG4B and is required for PLEKHG4B localization to cell–cell junctions (Ninomiya *et al.*, 2021). To further examine the role of ANXA2 binding in the junctional localization of PLEKHG4B, we first analyzed the ANXA2-binding region of PLEKHG4B. PLEKHG4B comprises an N-terminal Solo domain (a highly conserved domain in Solo and PLEKHG4B), a CRAL/TRIO domain and spectrin repeats in the central region, and a C-terminal DH-PH domain (Figure 3A). To determine the ANXA2-binding region of PLEKHG4B, we constructed Flag-tagged

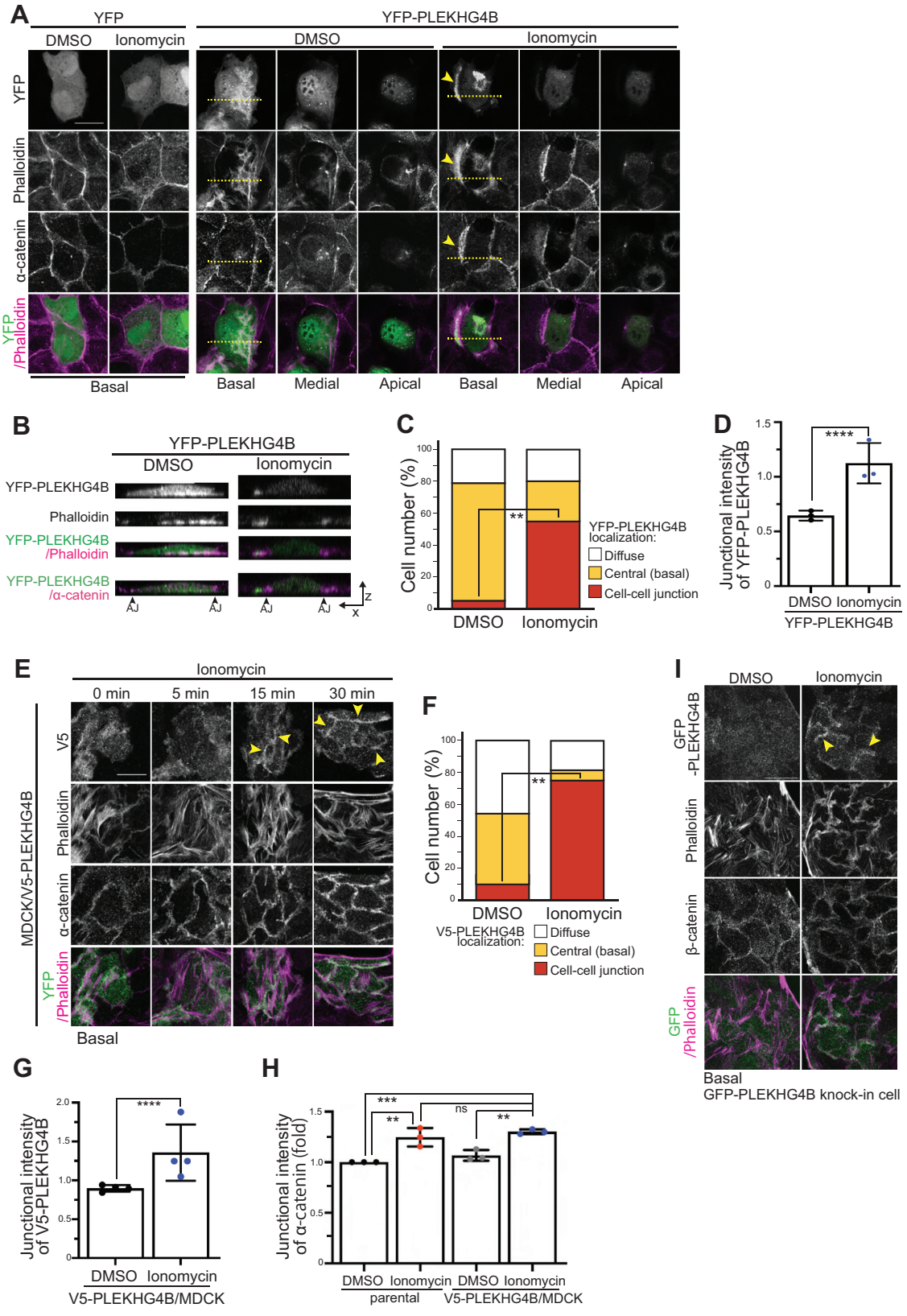


FIGURE 1: Calcium ionophore induces PLEKHG4B localization to cell–cell junctions. (A) Effects of ionomycin on the localization of YFP-PLEKHG4B. MDCK cells were transfected with YFP or YFP-PLEKHG4B, incubated for 24 h, and then treated with 2.5 μM ionomycin or control vehicle (DMSO) for 15 min. Cells were fixed and stained with rhodamine-phalloidin and anti-α-catenin antibody and imaged for YFP fluorescence. Single confocal sections at the basal, medial, and apical plane (0.65 and 1.3 μm upward from the basal plane, respectively) are shown. Merged images of YFP (green) and phalloidin (magenta) are shown in the bottom row. (B) The x-z images of the cells along a dashed yellow line in (A).

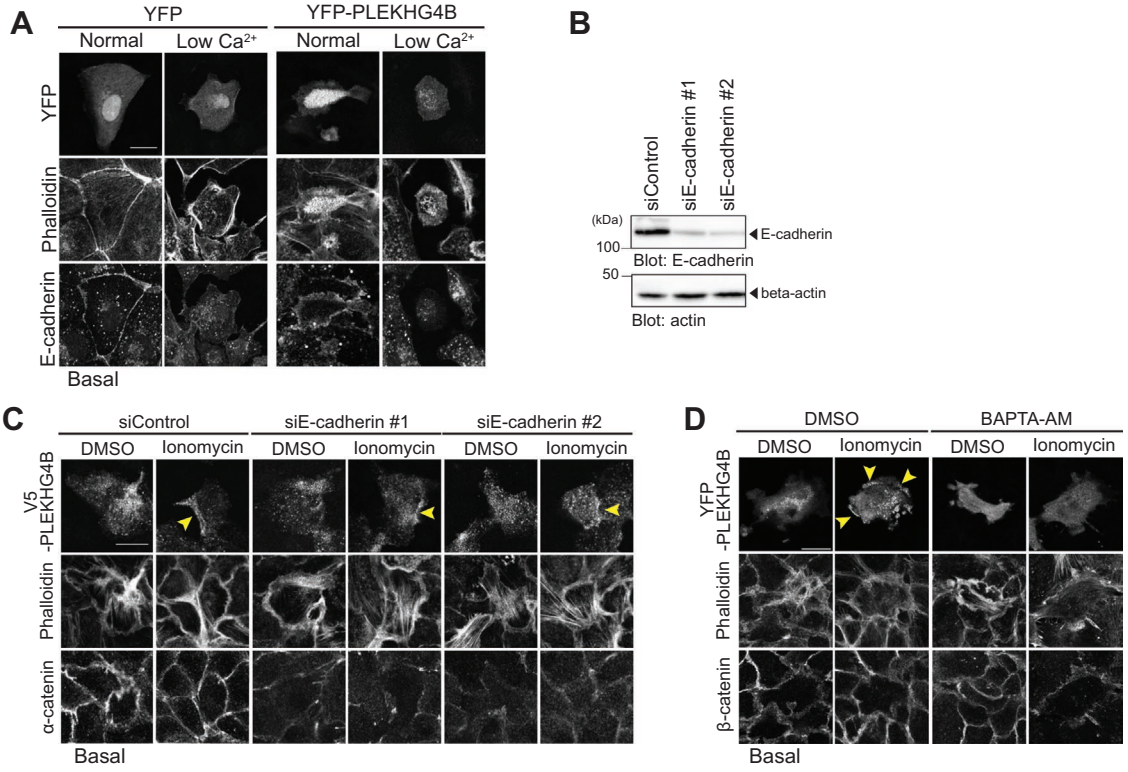


**FIGURE 2:** Effects of low $Ca^{2+}$ treatment or intracellular $Ca^{2+}$ chelation on PLEKHG4B localization. (A) Effects of low $Ca^{2+}$ on PLEKHG4B localization. MDCK cells were transfected with YFP or YFP-PLEKHG4B, incubated for 24 h in normal $Ca^{2+}$ medium, then cultured in normal or low $Ca^{2+}$ medium for 3 h. Cells were fixed and stained with rhodamine-phalloidin and anti-E-cadherin antibody. (B) Knockdown efficiency of E-cadherin-targeting siRNAs. MDCK cells were transfected with control or E-cadherin-targeting siRNAs and cultured for 48 h. Lysates were immunoblotted with anti-E-cadherin and anti-β-actin antibodies. (C) Effects of E-cadherin knockdown on PLEKHG4B localization. MDCK/V5-PLEKHG4B cells were transfected with control or E-cadherin-targeting siRNAs, cultured for 48 h, and then treated with 2.5 μM ionomycin or control DMSO for 15 min. Cells were fixed and stained with rhodamine-phalloidin and anti-V5 and anti-α-catenin antibodies. (D) Effects of BAPTA-AM on PLEKHG4B localization with or without ionomycin treatment. MDCK cells were transfected with YFP-PLEKHG4B and cultured for 48 h. Cells were treated with 10 nM BAPTA-AM for 15 min, followed by exposure to 2.5 μM ionomycin for 15 min. Then, cells were fixed, stained with rhodamine-phalloidin and anti-β-catenin antibody, and imaged for YFP fluorescence. In (A), (C), and (D), single confocal sections at the basal plane of the cells are shown. Yellow arrowheads indicate the positions of PLEKHG4B localization at cell–cell junctions. Scale bars: 20 μm.

(C) Quantification of the percentage of cells with diffuse, central, or cell–cell junctional localization of YFP-PLEKHG4B at the basal plane in ionomycin-untreated and -treated cells. (D) Quantification of the relative intensity of YFP-PLEKHG4B at cell–cell junctions to its intensity in the nonjunctional region at the basal plane. (E) Time-dependent changes in PLEKHG4B localization after ionomycin treatment. MDCK/V5-PLEKHG4B cells were cultured for 48 h to reach a subconfluent state and treated with 2.5 μM ionomycin. At the indicated times after ionomycin treatment, the cells were fixed and stained with rhodamine-phalloidin and anti-V5 and anti-α-catenin antibodies. Merged images are shown, as in (A). The single confocal sections at the basal plane of the cells are shown. (F) Quantification of the percentage of cells with diffuse, central, or cell–cell junctional localization of V5-PLEKHG4B at the basal plane with or without ionomycin treatment for 15 min. (G) Quantification of the relative intensity of V5-PLEKHG4B at cell–cell junctions to its intensity in the nonjunctional region at the basal plane. (H) Quantification of α-catenin intensity at cell–cell junctions at the basal plane. Relative intensity of α-catenin at cell–cell junctions was analyzed using ImageJ line scan analysis by taking the value in parental cells treated with DMSO set to 1.0. (I) Effects of ionomycin on the localization of GFP-PLEKHG4B in MDCK cells, in which GFP-PLEKHG4B was knocked-in into the 5′UTR of the PLEKHG4B gene locus. Cells were cultured for 48 h, treated with 2.5 μM ionomycin for 15 min, and then fixed and stained with rhodamine-phalloidin and anti-β-catenin antibody. Single confocal sections at the basal plane are shown. In (A), (E), and (I), yellow arrowheads indicate the positions of PLEKHG4B localization at cell–cell junctions. Scale bars: 20 μm. In (C) and (F), *P* values were calculated between the percentages of cells with junctional localization of PLEKHG4B by two-tailed paired *t* test, with over 32 cells from three independent experiments. In (D), (G), and (H), dot plot data are presented as the mean ± SD of three independent experiments, with over 15 cells evaluated in each experiment. *P* values were calculated using two-tailed paired *t* test (D and G) or ordinary one-way ANOVA followed by Dunnett's test (H). **, $P < 0.01$; ***, $P < 0.001$; ****, $P < 0.0001$; ns, not significant ($P > 0.05$).

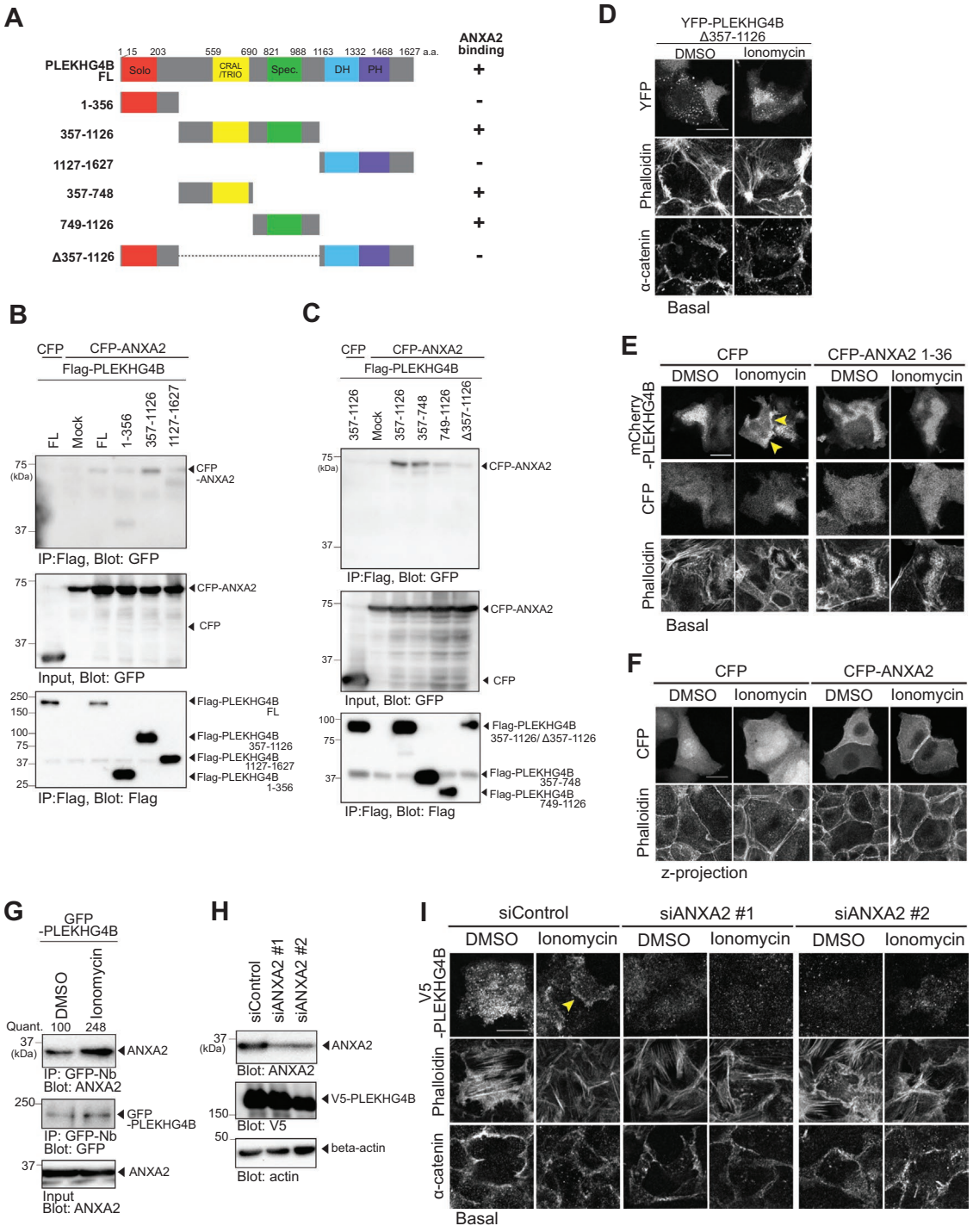


FIGURE 3: Annexin-A2 is required for ionomycin-induced PLEKHG4B localization to cell–cell junctions. (A) Schematic structure of human PLEKHG4B and its depletion mutants. Conserved domains are denoted by Solo, CRAL/TRIO, spectrin repeats (Spec), DH, and PH. The ANXA2-binding ability of each construct is indicated in the right. (B and C) Coimmunoprecipitation assays. HEK-293T cells coexpressing CFP-ANXA2 and Flag-PLEKHG4B or its deletion mutants were lysed and immunoprecipitated with anti-Flag antibody.IPs and lysates (Input) were analyzed by immunoblotting with anti-Flag or anti-GFP antibodies. (D) Effect of deletion of the central (357–1126) region on PLEKHG4B localization in ionomycin-treated and untreated cells. MDCK cells were transfected with YFP-PLEKHG4B (Δ357–1126), incubated for 24 h, and then treated with 2.5 μM ionomycin or vehicle for 15 min. Cells were fixed and stained with rhodamine-phalloidin and anti-α-catenin antibody. (E) Effects of overexpression of the N-terminal (1–36) fragment of ANXA2 on PLEKHG4B localization in ionomycin-treated and untreated cells. MDCK cells were cotransfected with CFP or CFP-ANXA2 (1–36) and mCherry-PLEKHG4B, incubated for 24 h, then treated with 2.5 μM ionomycin or vehicle for 15 min. Cells were fixed, stained with rhodamine-phalloidin, and imaged for CFP and mCherry fluorescence. (F) Effect of ionomycin on ANXA2 localization. MDCK cells were transfected with CFP or CFP-ANXA2 and cultured for 48 h. Cells were treated with 2.5 μM ionomycin or vehicle for 15 min, fixed, and stained with

full-length (FL) PLEKHG4B and its deletion mutants (Figure 3A); these were individually coexpressed with cyan fluorescent protein (CFP)-tagged ANXA2 in HEK-293T cells. Coimmunoprecipitation assays revealed that CFP-ANXA2 coprecipitated most efficiently with the central domain of PLEKHG4B (amino acids 357–1126), containing a CRAL/TRIO domain and spectrin repeats (Figure 3B; Supplemental Figure S3A). Moreover, CFP-ANXA2 was coprecipitated with PLEKHG4B(357–748) and (749–1126), but its coprecipitation was barely detectable with PLEKHG4B(Δ357–1126), which lacks the central region (Figure 3C; Supplemental Figure S3B). These results indicate that PLEKHG4B binds to ANXA2 primarily through the central (357–1126) region.

To examine the role of ANXA2 binding in PLEKHG4B localization, we analyzed the localization of PLEKHG4B(Δ357–1126) in vehicle- or ionomycin-treated cells. Similar to wild-type (WT) PLEKHG4B (shown in Figure 1A), PLEKHG4B(Δ357–1126) localized to the basal membrane in vehicle-treated cells (Figure 3D). However, unlike PLEKHG4B(WT), PLEKHG4B(Δ357–1126) did not accumulate at the cell–cell junctions but localized to the basal membrane even after ionomycin treatment (Figure 3D). These results suggest that the ANXA2-binding ability is required for ionomycin-induced localization of PLEKHG4B to the cell–cell junctions, but not for its localization to the basal membrane.

ANXA2 consists of an N-terminal cytosolic domain (amino acids 1–36) and a C-terminal $Ca^{2+}$- and membrane-binding domain (amino acids 37–339; Gerke *et al.*, 2005). We have previously shown that PLEKHG4B preferably binds to the N-terminal fragment of ANXA2 (Ninomiya *et al.*, 2021). To further examine the role of ANXA2 binding in PLEKHG4B localization, we examined the effect of overexpressing the N-terminal (1–36) fragment of ANXA2 on PLEKHG4B localization. MDCK cells were cotransfected with mCherry-tagged PLEKHG4B and CFP-tagged ANXA2(1–36) or control CFP, and then treated or untreated with ionomycin. When cotransfected with control CFP, mCherry-PLEKHG4B localized to the central region of the basal membrane without ionomycin and accumulated at the cell–cell junctions upon ionomycin treatment (Figure 3E). In contrast, cotransfection with CFP-ANXA2(1–36) suppressed ionomycin-induced junctional localization of PLEKHG4B, resulting in its localization to the basal membrane (Figure 3E). Furthermore, cotransfection with CFP-ANXA2(1–36) had no apparent effect on the basal membrane localization of PLEKHG4B in ionomycin-untreated cells. These results suggest that ANXA2(1–36) probably acts in a dominant-negative manner against endogenous ANXA2 and that binding to ANXA2 plays a crucial role in PLEKHG4B localization to the cell–cell junctions in response to ionomycin treatment, but it is not essential for its localization to the basal membrane in ionomycin-untreated cells.

We next examined the effect of ionomycin treatment on ANXA2 localization. MDCK cells transfected with CFP-tagged ANXA2 or control CFP were cultured for 48 h and then treated with ionomycin for 15 min. CFP-ANXA2 localized to the basal cell membrane and cell–cell junctions in ionomycin-untreated cells. Compared with this, ionomycin treatment markedly enhanced ANXA2 localization to the cell–cell junctions (Figure 3F). We also analyzed the effect of ionomycin treatment on the interaction between ANXA2 and PLEKHG4B by coimmunoprecipitation assay, using MDCK cells stably expressing GFP-PLEKHG4B. This assay revealed that ionomycin treatment markedly increased the amount of ANXA2 coprecipitated with GFP-PLEKHG4B (Figure 3G), indicating that ionomycin-induced $Ca^{2+}$ influx promotes the interaction between PLEKHG4B and ANXA2.

We further examined the effect of ANXA2 knockdown on PLEKHG4B localization in ionomycin-treated and -untreated cells. Suppression of ANXA2 expression was confirmed by immunoblot analysis (Figure 3H). As reported (Ninomiya *et al.*, 2021), ANXA2 knockdown suppressed PLEKHG4B localization to the cell–cell junctions in ionomycin-treated cells (Figure 3I). ANXA2 knockdown also suppressed PLEKHG4B localization to the basal membrane in ionomycin-treated and -untreated cells, resulting in its diffuse distribution (Figure 3I). These results suggest that ANXA2 is required for ionomycin-induced PLEKHG4B localization to the cell–cell junctions and also its localization to the basal membrane. On the other hand, we showed evidence above that ANXA2 binding is required for PLEKHG4B localization to cell–cell junctions but is not essential for its localization to the basal membrane. It is presumable that ANXA2 knockdown may have caused broader effects on other protein complex and machineries on the plasma membrane that indirectly affect membrane localization of PLEKHG4B. Expression of siRNA-resistant (sr) ANXA2 in ANXA2-knockdown cells recovered the inhibitory effect of ANXA2 knockdown on PLEKHG4B localization to the basal membrane (Supplemental Figure S3C), indicating that the inhibitory effect of ANXA2 siRNA treatment is caused by knockdown of ANXA2 but not due to the off-target effect. Expression of WT ANXA2 (which is downregulated by ANXA2-targeting siRNA) or its N-terminal fragment (1–36) in ANXA2-knockdown cells did not recover PLEKHG4B localization to the basal membrane, resulting in its diffuse distribution (Supplemental Figure S3C).

### The PH domain is involved in basal membrane localization of PLEKHG4B

The PH domain is generally known for its ability to bind to membrane phosphoinositides and to promote the membrane localization of many proteins (Snyder *et al.*, 2001). Within the PH domain, the $KX_n(K/R)XR$ sequence motif in the β1-β2 loop between the first two β-strands serves as a platform for phosphoinositide binding (Lemmon, 2008). To examine the role of the PLEKHG4B PH domain in its membrane localization, we constructed two YFP-tagged PLEKHG4B mutants, K1373A and K1373E, in which lysine-1373 in the consensus motif was replaced with alanine and glutamic acid, respectively (Figure 4A); we analyzed their localization in MDCK

rhodamine-phalloidin and imaged for CFP fluorescence. (G) Effect of ionomycin on the interaction between PLEKHG4B and ANXA2. MDCK cells stably-expressing GFP-PLEKHG4B were treated with 2.5 μM ionomycin or vehicle for 15 min, and lysates were immunoprecipitated with GFP-nanobody (GFP-Nb). IPs and lysates (Input) were analyzed by immunoblotting with anti-ANXA2 or anti-GFP antibodies. Quant.: relative immunoblot intensity of ANXA2 coprecipitated with GFP-PLEKHG4B is indicated. The relative intensity of ANXA2 in IP to Input is shown. (H) Knockdown efficiency of ANXA2-targeting siRNAs. MDCK/V5-PLEKHG4B cells were transfected with control or ANXA2-targeting siRNAs and cultured for 48 h. Lysates were immunoblotted with anti-ANXA2, anti-V5, and anti-β-actin antibodies. (I) Effect of ANXA2 knockdown on PLEKHG4B localization in ionomycin-treated and -untreated cells. MDCK/V5-PLEKHG4B cells were transfected with control or ANXA2-targeting siRNAs, cultured for 48 h, and then treated with 2.5 μM ionomycin or vehicle for 15 min. Cells were fixed and stained with rhodamine-phalloidin and anti-V5 and anti-α-catenin antibodies. In (D), (E), and (I), single confocal sections at the basal plane of the cells are shown. Yellow arrowheads indicate the positions of PLEKHG4B localization at cell–cell junctions. Scale bars: 20 μm.

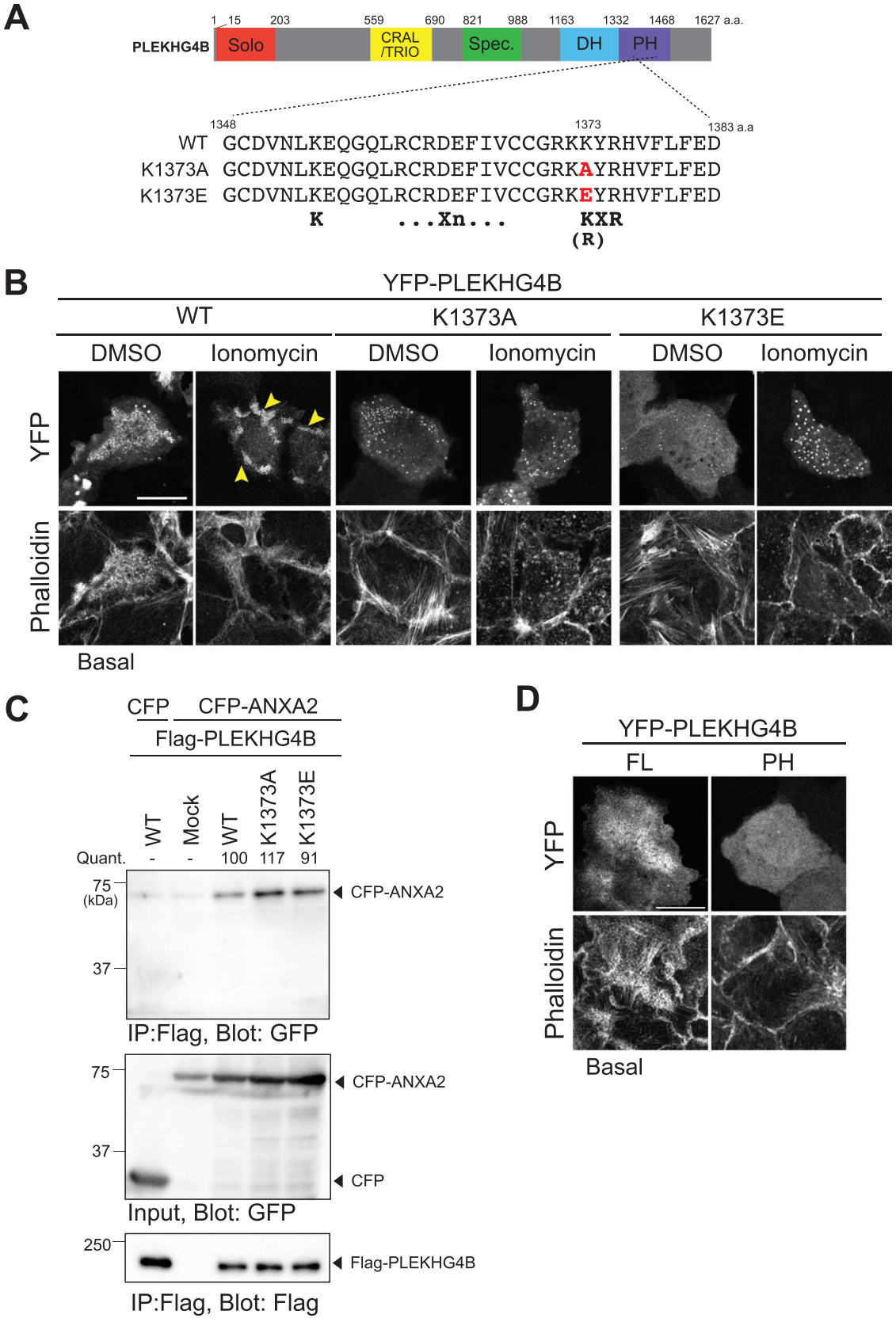


FIGURE 4: The PH domain is necessary but not sufficient for the basal membrane localization of PLEKHG4B. (A) Schematic structures of human PLEKHG4B and its PH domain mutants. The KXn(K/R)XR consensus motif for phosphoinositide binding is indicated at the bottom of the sequence. (B) Localization of the K1373A and K1373E mutants of PLEKHG4B in ionomycin-treated and untreated cells. MDCK cells were transfected with WT YFP-PLEKHG4B or its K1373A or K1373E mutant, incubated for 24 h, then treated with 2.5 μM ionomycin or vehicle for 15 min. Cells

cells. YFP-PLEKHG4B(WT) localized to the basal membrane in vehicle-treated cells and accumulated at cell–cell junctions in ionomycin-treated cells. In contrast, the K1373A and K1373E mutants neither localized to the basal membrane in vehicle-treated cells nor accumulated at cell–cell junctions in ionomycin-treated cells (Figure 4B). These results suggest that the phosphoinositide-binding activity of the PH domain is required for PLEKHG4B localization to the basal membrane in control cells and to the cell–cell junctions in ionomycin-treated cells. Coprecipitation assays revealed that CFP-ANXA2 was coprecipitated with each of the K1373A and K1373E mutants, at a level similar to that with PLEKHG4B(WT; Figure 4C), indicating that these mutants retain the ability to bind ANXA2. Thus, the phosphoinositide-binding activity of the PH domain, rather than the ANXA2-binding activity, is considered to be primarily involved in the basal membrane localization of PLEKHG4B, and the ANXA2-binding activity alone is not sufficient for ionomycin-induced junctional localization of PLEKHG4B. We also examined the localization of the YFP-tagged PH domain fragment (amino acids 1322–1495) of PLEKHG4B. The PH domain of PLEKHG4B was not localized to the basal membrane but diffusely distributed in the cytoplasm (Figure 4D), suggesting that the PH domain is necessary but not sufficient for the basal membrane localization of PLEKHG4B.

### $PI(4,5)P_2$ masking suppresses and its liberation recovers PLEKHG4B localization to the basal membrane

The PH domains bind to phosphoinositides, and ANXA2 binds to phosphatidylinositol-4,5-bisphosphate [$PI(4,5)P_2$] with high specificity (Snyder *et al.*, 2001; Rescher *et al.*, 2004; Gerke *et al.*, 2005). We therefore explored whether changes in the amount of $PI(4,5)P_2$ at the plasma membrane affect the localization of PLEKHG4B, using $PI(4,5)P_2$ masking/liberation and synthesis techniques (Ueno *et al.*, 2011). These techniques are based on rapamycin-induced complex formation of FK-506 binding protein (FKBP) with FKBP-rapamycin binding protein (FRB). In the $PI(4,5)P_2$ masking/liberation approach, $PI(4,5)P_2$ at the plasma membrane is masked by overexpression of the PH domain of phospholipase Cδ [PH(PLCδ)] conjugated with FKBP. FRB is targeted to the mitochondrial membrane by conjugation with the transmembrane motif of monoamine oxidase A (MoA), and rapamycin treatment induces translocation of FKBP-PH(PLCδ) to the mitochondria, thus liberating $PI(4,5)P_2$ at the plasma membrane (Figure 5A). When YFP-FKBP-PH(PLCδ) and CFP-FRB-MoA were coexpressed with control mCherry in MDCK cells, YFP-FKBP-PH(PLCδ) localized to the plasma membrane in vehicle-treated cells but was rapidly translocated to the mitochondria in response to rapamycin treatment (Figure 5B). When mCherry-PLEKHG4B was cotransfected with the $PI(4,5)P_2$ masking/liberation tools, it was diffusely distributed in the cytoplasm of control cells (Figure 5C), probably because $PI(4,5)P_2$ at the plasma membrane was masked by the overexpression of PH(PLCδ). In contrast, rapamycin treatment induced localization of mCherry-PLEKHG4B to the basal membrane, coincidentally with translocation of PH(PLCδ) to the mitochondria (Figure 5C). These results suggest that $PI(4,5)P_2$ at the plasma membrane plays a crucial role in PLEKHG4B localization to the basal membrane.

We also examined the effect of $PI(4,5)P_2$ masking on ionomycin-induced PLEKHG4B localization to cell–cell junctions. Masking of $PI(4,5)P_2$ by overexpression of mCherry-PH(PLCδ) suppressed ionomycin-induced PLEKHG4B localization to the cell–cell junctions, resulting in its diffuse distribution (Supplemental Figure S4A), which indicates that $Ca^{2+}$ influx alone does not trigger junctional localization of PLEKHG4B and that $PI(4,5)P_2$ is required for $Ca^{2+}$ influx-induced PLEKHG4B localization to cell–cell junctions as well as its localization to the basal membrane under normal $Ca^{2+}$ conditions. We also examined the effect of $Ca^{2+}$ depletion on $PI(4,5)P_2$-mediated PLEKHG4B localization to the basal membrane. The level of $PI(4,5)P_2$ at the plasma membrane was recovered upon rapamycin treatment in the $PI(4,5)P_2$ masking/liberation system (Figure 5A). Rapamycin-induced $PI(4,5)P_2$ liberation caused PLEKHG4B localization to the basal membrane but cotreatment with rapamycin and BAPTA-AM resulted in its diffuse distribution (Supplemental Figure S4B), indicating that elevation of $PI(4,5)P_2$ alone is not sufficient for PLEKHG4B localization to the basal membrane without $Ca^{2+}$.

We next used the $PI(4,5)P_2$ synthesis technique (Ueno *et al.*, 2011). In this approach, $PI(4,5)P_2$ was synthesized from phosphatidylinositol-4-phosphate [PI(4)P] by the enzyme activity of PI(4)P 5-kinase [PI(4)P5K]. Cells were cotransfected with FKBP-conjugated PI(4)P5K and the FRB-conjugated N-terminal sequence of Lyn kinase ($Lyn_{11}$), which targets FRB to the plasma membrane. Rapamycin treatment is predicted to induce FKBP-PI(4)P5K recruitment to the plasma membrane, thus increasing the amount of $PI(4,5)P_2$ at the plasma membrane (Figure 5D). When $Lyn_{11}$-CFP-FRB and YFP-FKBP-PI(4)P5K were coexpressed with control mCherry in MDCK cells, rapamycin treatment enhanced the localization of YFP-FKBP-PI(4)P5K to the plasma membrane (Figure 5E). When cells were cotransfected with mCherry-PLEKHG4B and the $PI(4,5)P_2$ synthesis tools, rapamycin treatment increased PLEKHG4B localization to the basal membrane and occasionally to the cell-cell junctions (Figure 5F), indicating that the increase in the amount of $PI(4,5)P_2$ at the plasma membrane enhanced PLEKHG4B localization to the basal membrane and cell–cell junctions.

It was reported that ionomycin induces $PI(4,5)P_2$ hydrolysis at the plasma membrane via activation of PLC in macrophage cells (Yeung *et al.*, 2006). We tested the effect of ionomycin on the level of $PI(4,5)P_2$ in MDCK cells, using GFP-PH(PLCδ) as a marker of $PI(4,5)P_2$. Ionomycin treatment had no apparent effect on the level of $PI(4,5)P_2$ at the plasma membrane in MDCK cells (Supplemental Figure S4C). A previous report also showed the existence of $PI(4,5)P_2$ at the plasma membrane after ionomycin treatment in MDCK cells (Evans *et al.*, 2006). Thus, it seems likely that ionomycin treatment does not significantly affect the level of $PI(4,5)P_2$ at the plasma membrane at least in MDCK cells.

were fixed and stained with rhodamine-phalloidin and imaged for YFP fluorescence. Yellow arrowheads indicate the positions of PLEKHG4B localization at cell-cell junctions. (C) Coimmunoprecipitation assays. HEK-293T cells coexpressing CFP-ANXA2 and Flag-PLEKHG4B or its K1473A or K1373E mutant were lysed and immunoprecipitated with anti-Flag antibody. IPs and lysates (Input) were analyzed by immunoblotting with anti-Flag or anti-GFP antibodies. Quant.: relative immunoblot intensity of CFP-ANXA2 bound to Flag-PLEKHG4B (WT or mutants) is indicated. The relative intensity of CFP-ANXA2 in IP to Input is shown. (D) Localization of the PH domain of PLEKHG4B. MDCK cells were transfected with YFP-PLEKHG4B full length (FL) or its PH domain (amino acids 1322–1495), incubated for 24 h, then fixed, stained with rhodamine-phalloidin and imaged for YFP fluorescence. In (B) and (D), single confocal sections at the basal plane of the cells are shown. Scale bars: 20 μm.

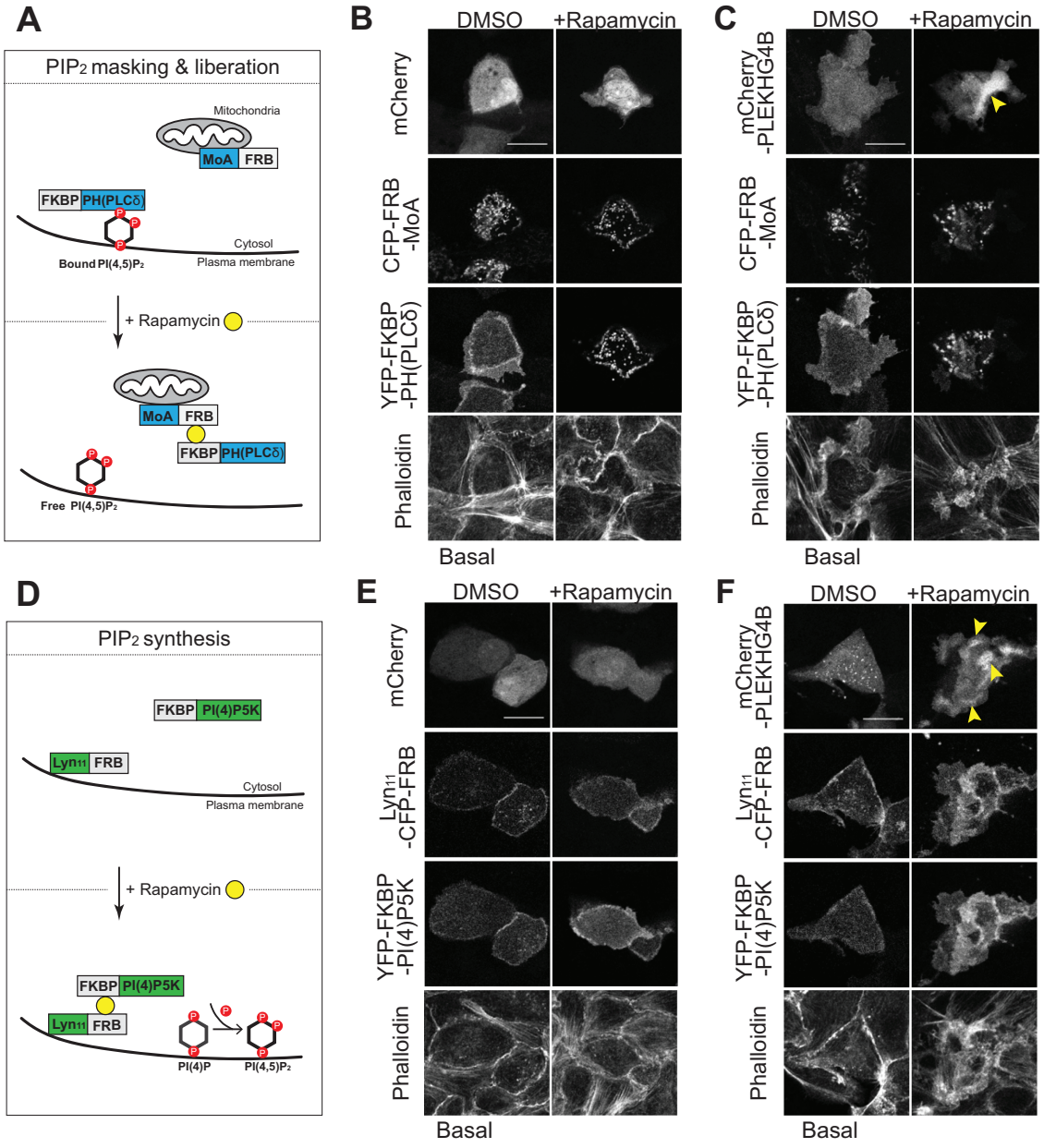


FIGURE 5: Effects of PI(4,5)$P_2$ masking, liberation, and synthesis on PLEKHG4B localization. (A) Schematic illustration of PI(4,5)$P_2$ masking and liberation technique. In the absence of rapamycin, FKBP-PH(PLCδ) masks PI(4,5)$P_2$ at the plasma membrane. Rapamycin treatment induces FKBP-PH(PLCδ) translocation to the mitochondrial membrane by binding to CFP-FRB-MoA, thereby enabling PI(4,5)$P_2$ liberation at the plasma membrane. (B and C) Effects of PI(4,5)$P_2$ masking and liberation on PLEKHG4B localization. MDCK cells were cotransfected with CFP-FRB-MoA, YFP-FKBP-PH(PLCδ), and mCherry (B) or mCherry-PLEKHG4B (C). Cells were cultured for 24 h, then treated with 100 nM rapamycin or vehicle for 15 min. Cells were fixed and stained with rhodamine-phalloidin and imaged for mCherry, CFP, and YFP. (D) Schematic illustration of PI(4,5)$P_2$ synthesis technique. In the absence of rapamycin, FKBP-PI(4)P5K localizes in the cytosol, but rapamycin treatment induces FKBP-PI(4)P5K recruitment to the plasma membrane by binding to Lyn11-FRB, thus promoting PI(4,5)$P_2$ synthesis at the plasma membrane. (E and F) Effects of PI(4,5)$P_2$ synthesis on PLEKHG4B localization. MDCK cells were cotransfected with Lyn11-CFP-FRB, YFP-FKBP-PI(4)P5K, and mCherry (E) or mCherry-PLEKHG4B (F), and analyzed as in (B) and (C). In (B), (C), (E), and (F), single confocal sections at the basal plane of the cells are shown. Yellow arrowheads indicate the basal membrane localization of PLEKHG4B. Scale bars: 20 μm.

### MSCs are involved in PLEKHG4B localization

Ionomycin treatment is an artificial system for investigating the role of calcium influx in various cell responses. To explore whether any physiological stimuli that induce calcium influx could affect PLEKHG4B localization, we next analyzed the effects of mechanical force-induced calcium influx on PLEKHG4B localization. Recent studies have shown that the MSC-mediated $Ca^{2+}$ influx is involved in regulating cell–cell junctional actin organization and cell–cell junction integrity (Rajakylä *et al.*, 2020; Efremov *et al.*, 2022; Yao *et al.*, 2022). To examine the role of MSCs in PLEKHG4B localization, we first analyzed the effects of Yoda1 and Jedi2 (selective activators of Piezo1 mechanosensitive channel) on the localization of PLEKHG4B.

Live imaging analyses of MDCK cells stably expressing GCaMP6 revealed that treatment with Yoda1 caused rapid increase in intracellular $Ca^{2+}$ and the high level of $Ca^{2+}$ was maintained until 15 min after Yoda1 treatment (Supplemental Figure S5A), confirming that activation of Piezo1 induces $Ca^{2+}$ influx in MDCK cells. When MDCK cells expressing YFP-PLEKHG4B were treated with Yoda1 or Jedi2, PLEKHG4B accumulated at the cell–cell junctions with concomitant accumulation of actin filaments at the PLEKHG4B-enriched region (Figure 6, A–C), a phenotype similar to that observed after ionomycin treatment (shown in Figure 1, A–C). Additionally, Yoda1 treatment induced GFP-PLEKHG4B localization to cell–cell junctions in GFP-PLEKHG4B knock-in cells (Supplemental Figure S5B). Yoda1-induced PLEKHG4B localization to the cell–cell-junctions was abrogated in low $Ca^{2+}$ medium or by pretreatment with BAPTA-AM (Supplemental Figure S5, C and D). These results suggest that Piezo1-mediated $Ca^{2+}$ influx promotes PLEKHG4B localization to cell–cell junctions. We also examined the effect of GSK1016790A (a selective activator of TRPV4) on PLEKHG4B localization, but as more than 90% of the cells were rounded up after treatment with this reagent even at a concentration of 10 nM, its effect could not be determined.

We next examined the effect of GsMTx4 (an inhibitor of several MSCs, including the TRP family and Piezo channels) on the localization of PLEKHG4B. MDCK cells expressing YFP-PLEKHG4B were treated with GsMTx4 or control DMSO for 15 min. PLEKHG4B mostly localized to the basal membrane in control cells, but treatment with GsMTx4 suppressed its localization to the basal membrane (Figure 6, D and E), suggesting that MSCs-mediated $Ca^{2+}$ influx is involved in PLEKHG4B localization to the basal membrane under normal $Ca^{2+}$ culture conditions.

Recent studies indicate that the MSC-mediated $Ca^{2+}$ influx regulates cell-cell junctional actin reorganization through the $Ca^{2+}$/calmodulin-dependent kinase kinase 2 (CaMKK2) and AMP-activated protein kinase (AMPK) signaling pathways (Tojkander *et al.*, 2018; Rajakylä *et al.*, 2020). Thus, we examined whether these enzymes are involved in PLEKHG4B localization. Treatments with AICAR (an activator of AMPK), compound C (an inhibitor of AMPK), or STO-609 (an inhibitor of CaMKKs) had no apparent effect on PLEKHG4B localization at the basal membrane in ionomycin-untreated cells and its accumulation at the cell–cell junctions in ionomycin-treated cells (Supplemental Figure S6). Thus, the localization of PLEKHG4B to the basal membrane and cell–cell junctions is regulated by intracellular $Ca^{2+}$ concentration, but is independent of the CaMKK2-AMPK signaling pathway.

### Inhibition of MSCs or intracellular $Ca^{2+}$ chelation impairs the integrity of actin organization at cell–cell junctions

We have previously shown that knockdown of PLEKHG4B attenuates E-cadherin localization to cell–cell junctions and delays the maturation of cell–cell adhesions, indicating that PLEKHG4B is involved in the formation and maintenance of cell–cell adhesions (Ninomiya *et al.*, 2021). In this study, we analyzed the effects of PLEKHG4B knockdown on actin and α-catenin organization at the cell–cell junctions in MDCK cells. The cells were treated with two independent siRNAs targeting PLEKHG4B or control siRNA, cultured for 48 h, and then fixed and stained with rhodamine-phalloidin and with anti-α-catenin (as an adherens junction marker) and anti-ZO-1 antibodies (as a tight junction marker). The PLEKHG4B-targeting siRNAs effectively suppressed the expression of PLEKHG4B transcripts in MDCK cells (Figure 7B). Confocal microscopic analyses at the basal plane revealed that actin filaments mostly localized at the cell–cell junctions and aligned along the cell–cell boundary in control siRNA-treated cells. In contrast, actin filaments were more broadly distributed in the region away from the cell–cell contact sites and the ventral stress fibers on the basal plane of the cell increased in PLEKHG4B knockdown cells (Figure 7A). Line scanning of fluorescence signals from actin filaments across the cell–cell contact sites revealed that PLEKHG4B knockdown induced broader distribution of actin filaments in the region away from the cell–cell contact sites (Figure 7C). To quantitate the distribution of actin filaments, we analyzed the relative fluorescence intensity of rhodamine-phalloidin staining in the region of every 2 μm width from the cell–cell contact site, with that in the region of 0–2 μm set as 1.0. The relative intensity of actin filaments in the region of 2–4 μm in PLEKHG4B knockdown cells was significantly higher than that in control cells (Figure 7D), indicating that actin filaments were tightly packed at cell–cell junctions in control cells but they became more broadly distributed in PLEKHG4B knockdown cells. We also analyzed the fluorescence intensity of α-catenin at the cell–cell junctions. Quantitative analyses showed that PLEKHG4B knockdown significantly decreased the intensity of α-catenin signals at the cell–cell junctions (Figure 7E). Thus, in accordance with our previous results (Ninomiya *et al.*, 2021), these observations indicate that PLEKHG4B is required for the proper accumulation and organization of actin filaments and α-catenin at cell–cell junctions. Additionally, z-stack imaging showed that PLEKHG4B knockdown had no apparent effect on ZO-1 staining (Figure 7A).

To explore the role of MSC and intracellular $Ca^{2+}$ signaling in cell–cell junction integrity, we analyzed the effects of GsMTx4 or BAPTA-AM on actin and α-catenin organization at the cell–cell junctions. MDCK cells cultured in a confluent monolayer were treated with GsMTx4 or BAPTA-AM, then fixed and stained with rhodamine-phalloidin and with anti-α-catenin and anti-ZO-1 antibodies. Treatments with GsMTx4 or BAPTA-AM induced broad distribution of actin filaments away from the cell–cell contact site and an increase in ventral stress fibers at the basal membrane of the cell (Figure 7 F–H). Moreover, treatments with GsMTx4 or BAPTA-AM attenuated the fluorescence intensity of α-catenin at the cell–cell junctions (Figure 7I). Thus, treatments with GsMTx4 or BAPTA-AM impaired actin filament accumulation in the confined zone of cell–cell adhesions and decreased the amount of α-catenin at the cell–cell junctions, phenotypes similar to those observed in PLEKHG4B-knockdown cells. These results suggest that MSC-mediated $Ca^{2+}$ influx and intracellular $Ca^{2+}$ signaling are required for the proper accumulation and organization of actin filaments and α-catenin at cell–cell junctions.

## DISCUSSION

In this study, we provide evidence that intracellular $Ca^{2+}$ signals regulate PLEKHG4B localization to the basal membrane and cell–cell junctions. PLEKHG4B localized to the basal membrane in normal $Ca^{2+}$ medium, but ionomycin treatment induced accumulation of PLEKHG4B and actin filaments at cell–cell junctions, indicating that ionomycin-induced $Ca^{2+}$ influx triggers PLEKHG4B localization to cell–cell junctions, thereby inducing junctional actin cytoskeleton remodeling. Low $Ca^{2+}$ treatment suppressed PLEKHG4B localization to the basal membrane and caused its diffuse distribution in the cytoplasm. Knockdown of E-cadherin disrupted cell–cell adhesions but did not affect the basal membrane localization of PLEKHG4B, indicating that low $Ca^{2+}$ treatment impairs basal membrane localization of PLEKHG4B by decreasing intracellular $Ca^{2+}$, but not by disrupting E-cadherin-mediated cell–cell adhesions. Treatment with an intracellular $Ca^{2+}$ chelator BAPTA-AM suppressed PLEKHG4B localization either to the basal membrane under normal $Ca^{2+}$ conditions

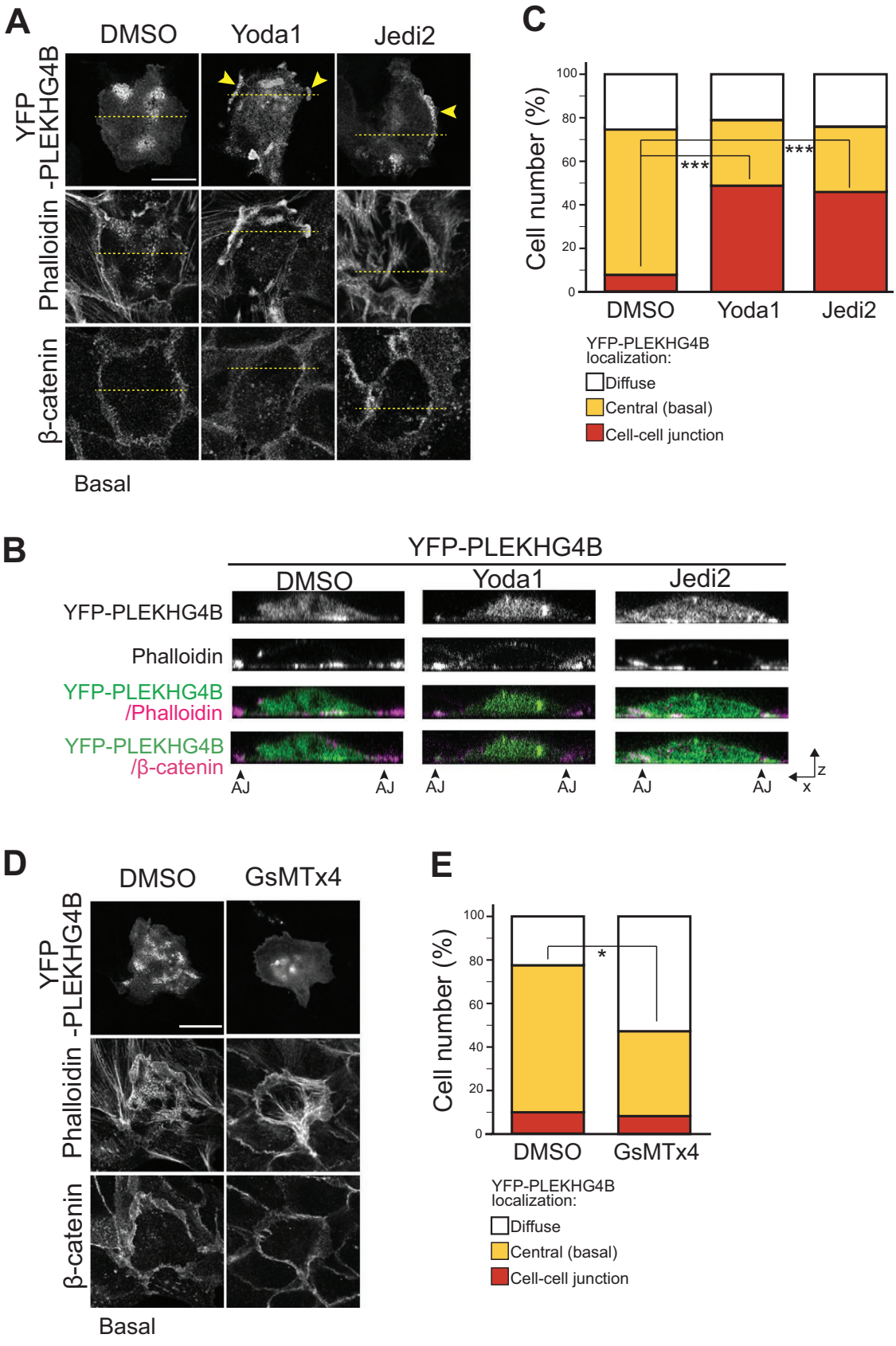


FIGURE 6: MSCs are involved in PLEKHG4B localization to basal membranes and cell-cell junctions. (A) Treatment with Yoda1 or Jedi2 promotes PLEKHG4B localization to cell-cell junctions. MDCK cells were transfected with YFP-PLEKHG4B, cultured for 24 h, and then treated with 10 μM Yoda1, 50 μM Jedi2, or vehicle for 15 min. Cells were fixed and stained with rhodamine-phalloidin and anti-β-catenin antibodies. (B) The x-z images of the cells along a dashed

or to cell–cell junctions after ionomycin treatment. Together, these findings suggest that the intracellular $Ca^{2+}$ concentration is a key factor in regulating PLEKHG4B localization; it diffusely distributes in the cytoplasm under low $Ca^{2+}$ conditions, localizes to the basal membrane under normal $Ca^{2+}$ conditions, and accumulates at the cell–cell junction under higher $Ca^{2+}$ conditions (Figure 8).

ANXA2 is a $Ca^{2+}$- and phosphoinositide-binding protein that mediates membrane localization of many proteins (Gerke *et al.*, 2005). We have previously shown that ANXA2 binds to PLEKHG4B and that ANXA2 knockdown suppresses PLEKHG4B localization to cell–cell junctions (Ninomiya *et al.*, 2021). Deletion of the ANXA2-binding region of PLEKHG4B or overexpression of the N-terminal PLEKHG4B-binding fragment of ANXA2 also suppressed ionomycin-induced PLEKHG4B localization to cell–cell junctions, but had no apparent effect on its localization to the basal membrane in ionomycin-untreated cells. In addition, ionomycin treatment promoted ANXA2 localization to cell–cell junctions. These results strongly suggest that association with ANXA2 plays a critical role in ionomycin-induced PLEKHG4B localization to cell–cell junctions, but has no apparent role in its basal membrane localization under normal $Ca^{2+}$ conditions. Previous studies have shown that ANXA2 binds to membrane phospholipids, preferentially to $PI(4,5)P_2$, in a $Ca^{2+}$-dependent manner, and recruits actin regulatory proteins, such as Rac1, Cdc42, and Tuba (a Cdc42-targeting GEF), to the confined area of the plasma membrane, thereby inducing actin reorganization underneath the plasma membrane (Ikebuchi and Waisman, 1990; Hansen *et al.*, 2002; Gerke *et al.*, 2005; Yamada *et al.*, 2005; Martin-Belmonte *et al.*, 2007; Bryant *et al.*, 2010; Bharadwaj *et al.*, 2013). Our results suggest that ANXA2 also plays a functional role in regulating actin cytoskeletal remodeling at cell–cell junctions through $Ca^{2+}$-dependent recruitment of PLEKHG4B to cell–cell junctions.

We have shown evidence that ANXA2 binding is required for PLEKHG4B localization to cell–cell junctions, but not for its localization to the basal membrane. On the other hand, ANXA2 knockdown suppressed PLEKHG4B localization to the basal membrane as well as its localization to cell–cell junctions. These apparently contradictory results could be due to the broader destructive effects of ANXA2 knockdown on membrane structures and compositions that indirectly affect membrane localization of PLEKHG4B. ANXA2 localized at cell–cell junctions in ionomycin-untreated cells, albeit to a lesser extent than that in ionomycin-treated cells. Nonetheless, there was no PLEKHG4B at cell–cell junctions in ionomycin-untreated cells, indicating that the junctional localization of ANXA2 is not sufficient for PLEKHG4B localization to cell–cell junctions. Because the ionomycin treatment increased the interaction between PLEKHG4B and ANXA2, it is conceivable that ionomycin-induced $Ca^{2+}$ influx leads to PLEKHG4B recruitment to cell–cell junctions via affecting the states of ANXA2 protein complexes or junctional membrane structures and thereby enhancing the binding ability of ANXA2 to PLEKHG4B.

We also demonstrate that the phosphoinositide-binding activity of the PH domain of PLEKHG4B is required for its localization to the basal membrane and cell–cell junctions. The mutation of Lys-1373 in the phosphoinositide-binding consensus motif of the PH domain severely impairs PLEKHG4B localization to the basal membrane in normal $Ca^{2+}$ medium and to cell–cell junctions after ionomycin treatment. As these mutants retained binding ability to ANXA2, their defect in localization was caused by the loss of phospholipid-binding ability, but not by the loss of the ANXA2-binding ability. Thus, it is likely that the direct binding of the PH domain to phosphoinositides is a prerequisite for PLEKHG4B localization to the basal membrane and cell–cell junctions, while ANXA2 plays a principal role in its $Ca^{2+}$ influx-induced localization to cell–cell junctions.

Using $PI(4,5)P_2$ masking/liberation techniques (Ueno *et al.*, 2011), we showed that $PI(4,5)P_2$ masking suppresses the basal membrane localization of PLEKHG4B, whereas its liberation recovers it. The $PI(4,5)P_2$ synthesis technique showed that the increased $PI(4,5)P_2$ in the plasma membrane enhances PLEKHG4B localization to the basal membrane and cell–cell junctions. These results suggest that $PI(4,5)P_2$ plays a crucial role in PLEKHG4B localization to the basal membrane and cell–cell junctions. $PI(4,5)P_2$ is known to regulate actin filament dynamics at the plasma membrane by binding to numerous actin regulators (Ueno *et al.*, 2011; Janmey *et al.*, 2018). Our results suggest that $PI(4,5)P_2$ also serves to regulate actin filament remodeling underneath the plasma membrane by recruiting PLEKHG4B to the defined area of the plasma membrane. As ANXA2 binds to $PI(4,5)P_2$ with high specificity (Rescher *et al.*, 2004; Gerke *et al.*, 2005), it is plausible that PLEKHG4B binds to $PI(4,5)P_2$ in two ways: direct binding via its PH domain and indirect binding via its central region through the ANXA2-$Ca^{2+}$ complex (Figure 8). We also showed that neither ionomycin treatment without $PI(4,5)P_2$ nor elevation of $PI(4,5)P_2$ without $Ca^{2+}$ caused PLEKHG4B localization to the basal membrane. Collectively, our results suggest that PLEKHG4B localization to the basal membrane requires both appropriate levels of intracellular $Ca^{2+}$ and the $PI(4,5)P_2$-binding ability of the PH domain, while its localization to cell–cell junctions requires high levels of intracellular $Ca^{2+}$, the $PI(4,5)P_2$-binding ability of the PH domain, and the ANXA2-binding of the central region (Figure 8).

Calcium signaling plays crucial roles in diverse cell activities, including actin cytoskeletal dynamics and remodeling. Recent studies have shown that MSC-mediated $Ca^{2+}$ influx regulates actin filaments dynamics at the cell–cell junctions and cell-matrix adhesions (Ko *et al.*, 2001; Hashido *et al.*, 2006; Rajakylä *et al.*, 2020; Varadarajan *et al.*, 2022; Yao *et al.*, 2022). In this study, we showed that treatment with Yoda1 and Jedi2 (activators of Piezo1) promote PLEKHG4B localization to cell–cell junctions and treatment with GsMTx-4 (an inhibitor of several MSCs) suppresses its localization to the basal membrane. These results suggest that MSC-mediated $Ca^{2+}$ influx is involved in PLEKHG4B localization to the basal membrane and cell–cell junctions. Treatments with GsMTx-4 or BAPTA-AM also affect

yellow line in (A). (C) Quantification of the percentage of cells with diffuse, central, or cell-cell junctional localization of YFP-PLEKHG4B at the basal plane in Yoda1- or Jedi2-treated cells. (D) Effects of GsMTx4 on PLEKHG4B localization to the basal membrane. MDCK cells were transfected with YFP-PLEKHG4B, cultured for 48 h, and then treated with 10 μM GsMTx4 or vehicle for 15 min. Cells were fixed and stained with rhodamine-phalloidin and anti-β-catenin antibody. (E) Quantification of the percentage of cells with diffuse, central, or cell–cell junctional localization of YFP-PLEKHG4B at the basal plane in GsMTx4-treated and -untreated cells. In (A) and (D), single confocal sections at the basal plane of the cells are shown. Yellow arrowheads indicate the positions of PLEKHG4B localization at cell–cell junctions. Scale bars: 20 μm. In (C) and (E), *P* values were calculated by ordinary one-way ANOVA followed by Dunnett's test (C) or two-tailed paired *t* test (E), with over 25 cells from three independent experiments. *, $P < 0.05$; ***, $P < 0.001$.

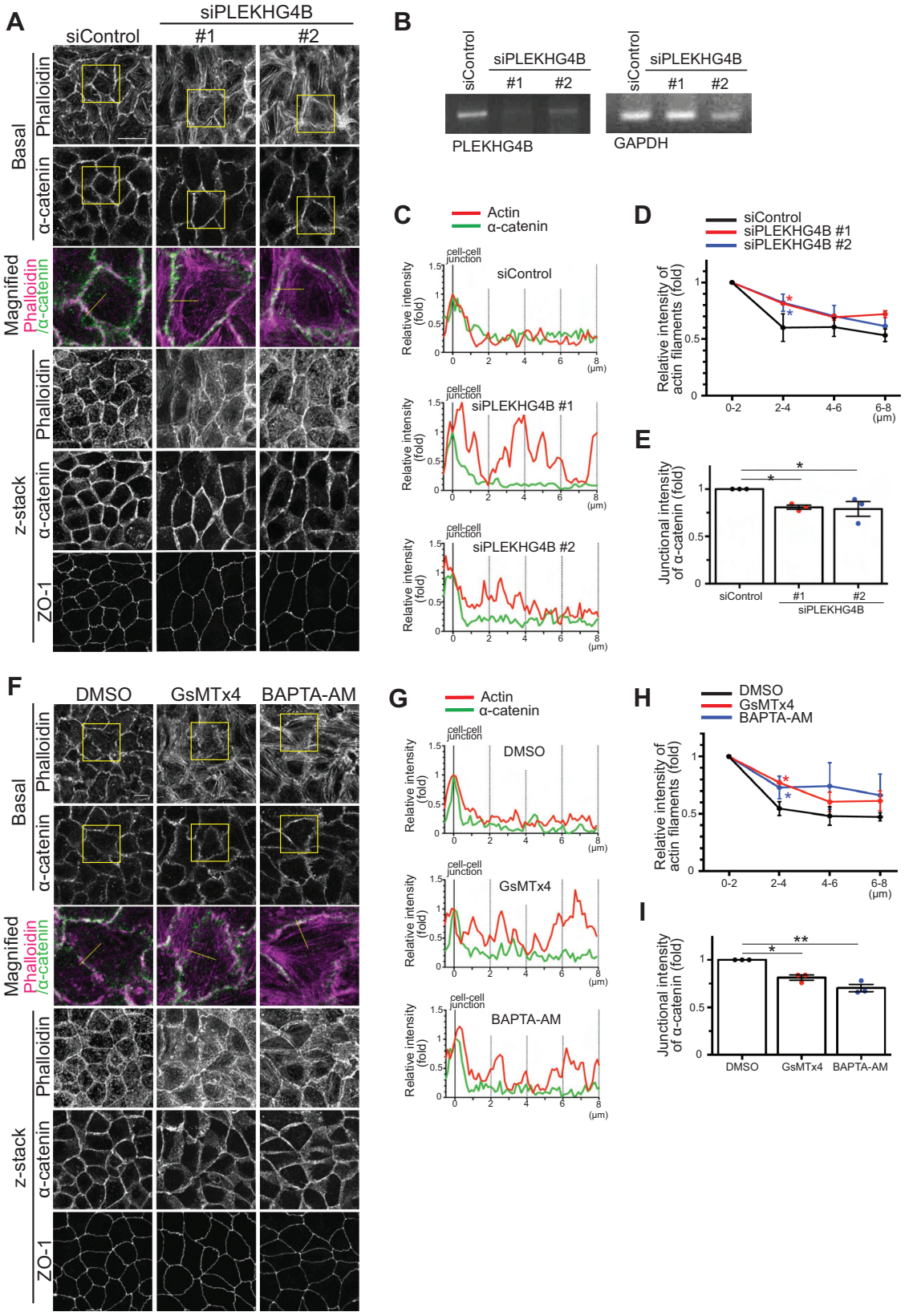


FIGURE 7: PLEKHG4B knockdown, inhibition of mechanosensitive channel, or intracellular $Ca^{2+}$ chelation affects actin organization at cell–cell junctions. (A) Effects of PLEKHG4B knockdown on actin filament organization at cell–cell junctions. MDCK cells were transfected with control or PLEKHG4B siRNAs and cultured for 48 h. Cells were fixed and stained with rhodamine-phalloidin and anti-α-catenin and anti-ZO-1 antibodies. Magnified images of the boxed regions are shown. (B) Knockdown efficiency of PLEKHG4B-targeting siRNAs. MDCK cells were transfected with control or PLEKHG4B-targeting siRNAs and cultured for 48 h. Total RNA was isolated and subjected to semiquantitative RT-PCR.

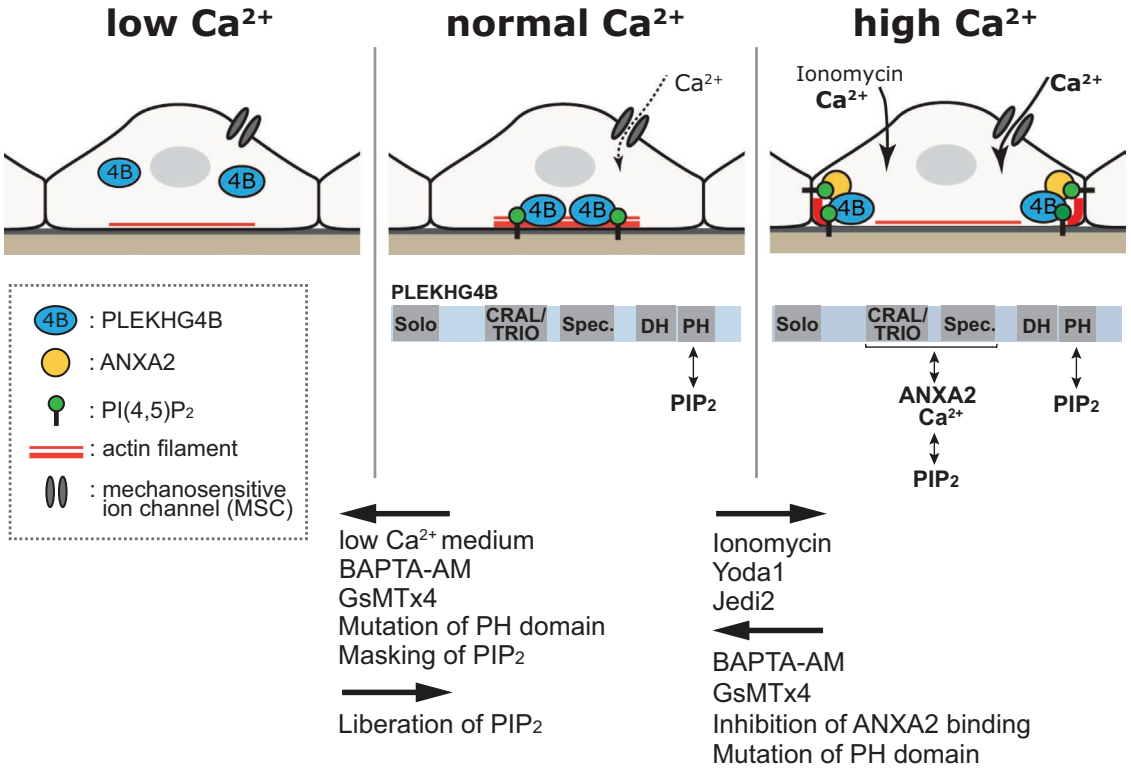


**FIGURE 8:** Proposed model for the role of $Ca^{2+}$ influx, $PI(4,5)P_2$, ANXA2, and MSCs in PLEKHG4B localization. PLEKHG4B localizes to the basal membrane in normal $Ca^{2+}$ medium. Ionomycin treatment causes PLEKHG4B accumulation at cell–cell junctions. Ionomycin-induced PLEKHG4B localization at cell–cell junctions is suppressed by treatment with BAPTA-AM, inhibition of its binding to ANXA2 or $PI(4,5)P_2$, indicating that $Ca^{2+}$ influx and association with ANXA2 and $PI(4,5)P_2$ are required for junctional localization of PLEKHG4B. Treatment with low $Ca^{2+}$ or BAPTA-AM or inhibition of $PI(4,5)P_2$ binding suppresses PLEKHG4B localization to the basal membrane in normal $Ca^{2+}$ medium, indicating that the suitable level of $Ca^{2+}$ and $PI(4,5)P_2$-binding are required for its basal membrane localization. Yoda1 and Jedi2 promote PLEKHG4B localization to cell–cell junctions and GsMTx4 suppresses its localization to cell–cell junctions and the basal membrane, indicating that MSC-mediated $Ca^{2+}$ influx is involved in PLEKHG4B localization to these regions. See text for details.

the organization of actin filaments and α-catenin at the cell–cell junctions. Actin bundles were tightly packed along the cell–cell contacts in control cells, but in cells treated with GsMTx4 or BAPTA-AM, they were more broadly distributed in the region away from the cell–cell contacts and the ventral stress fibers increased. Moreover, α-catenin signals at cell–cell contacts decreased after GsMTx4 or BAPTA-AM treatment. These results suggest that MSC-mediated $Ca^{2+}$ influx plays a crucial role in actin cytoskeletal remodeling at cell–cell junctions and in the integrity of cell–cell adhesions. Notably, the phenotypes of GsMTx4- or BAPTA-AM-treated cells were

(C) Line scans of the fluorescence intensity of actin filaments (red) and α-catenin (green) across the cell–cell junction area on the basal plane along the yellow lines in the magnified images in (A). The position showing the intensity peak of α-catenin is set as 0 μm. Fluorescent intensity of F-actin or α-catenin at 0 μm is set to 1.0. (D) Quantification of fluorescence intensity of actin filaments across the cell–cell junction area on the basal plane. The line was randomly drawn perpendicular to the cell–cell junctional site. The line length was 8 μm and set 0 μm at the intensity peak of α-catenin considered as cell–cell contact site. For every 2 μm, the average fluorescence intensity was calculated. Data are expressed as the mean ± SD of three independent experiments, with 24 junctions evaluated in each experiment. *P* values were calculated by ordinary one-way ANOVA followed by Dunnett's test. (E) Quantification of α-catenin intensity at cell–cell junctions in z-stack images. Relative intensity of α-catenin at cell–cell junctions was analyzed using ImageJ line scan analysis by taking the value in control cells set to 1.0. Data represent mean ± SD of three independent experiments, with 30 cell–cell contacts per experiment. *P* values were calculated as in (D). (F) Effects of GsMTx4 or BAPTA-AM treatment on actin filament organization at cell–cell junctions. MDCK cells were cultured for 48 h to form a confluent monolayer and treated with 10 μM GsMTx4 for 16 h or 25 nM BAPTA-AM for 15 min. Cells were fixed and analyzed as in (A). (G) Line scans of the fluorescence intensity of actin filaments (red) and α-catenin (green) along the yellow lines in the magnified images in (F). Relative intensity was analyzed as in (C). (H) Quantification of fluorescence intensity of actin filaments at cell–cell junction area on the basal plane. Average intensity was analyzed as in (D). (I) Quantification of α-catenin intensity at cell–cell junctions in z-stack images. Relative intensity was analyzed as in (E). *, $P < 0.05$; **, $P < 0.01$. Scale bars: 20 μm.

closely related to those observed in PLEKHG4B-knockdown cells. Thus, it is plausible that MSC-mediated $Ca^{2+}$ influx stimulates PLEKHG4B localization to cell–cell junctions, thereby leading to actin remodeling at cell–cell junctions and supporting the integrity of cell–cell adhesions. Rajakylä *et al.* (2020) recently reported similar results that GsMTx4 treatment leads to loss of peripheral actomyosin bundles and appearance of ventral stress fibers. They also showed that the assembly of peripheral actomyosin bundles is dependent on the CaMKK2-AMPK signaling pathway. However, activation or inhibition of CaMKK2 or AMPK had no apparent effect on the junctional localization of PLEKHG4B in our experiments, indicating that PLEKHG4B localizes to cell–cell junctions, independently of the CAMKK2-AMPK pathway. It is possible that MSC-mediated $Ca^{2+}$ influx induces local accumulation of ANXA2, which serves to recruit and tether PLEKHG4B to the cell–cell junctions thereby inducing actin filament assembly at cell–cell junctions. Additionally, a recent study has shown that activation of TRPV4, a member of mechanosensitive $Ca^{2+}$ channels, promotes Cdc42 activation along with cell migration and invasion in glioblastoma cells (Yang *et al.*, 2020). As PLEKHG4B is a Cdc42-targeting GEF, PLEKHG4B might be involved in these cell responses.

Epithelial cells in sheets are continuously exposed to mechanical forces at cell–cell junctions with adjacent cells and at the cell-matrix interface. Cells sense and respond to changes in these circumstantial mechanical cues for the maintenance and remodeling of cell–cell and cell-matrix adhesions by regulating junctional actin cytoskeletal organization. In this study, we provide evidence that MSCs-mediated $Ca^{2+}$ influx is involved in PLEKHG4B localization to the basal membrane and cell–cell junctions and actin filament assembly at these adhesion sites. Our results provide new insights into the relationship between MSCs-mediated $Ca^{2+}$ influx and actin cytoskeletal remodeling at cell–cell and cell-matrix adhesions. Further studies are needed to better understand the mechanisms allowing cells to respond to mechanical signals for controlling dynamics and remodeling of cell–cell and cell-matrix adhesions.

## MATERIALS AND METHODS

Request a protocol through *Bio-protocol*.

### Reagents and antibodies

Ionomycin (I24222) was obtained from Thermo Fisher Scientific. BAPTA-AM (SC119) was obtained from DOJINDO. Yoda1 (21906), GSK1016790A (17289), and STO-609 (15325) were obtained from Cayman Chemical. Jedi2 (HY-131018) was obtained from MedChem Express. GsMTx-4 (4939-s) was obtained from Peptide Institute. Compound C (17126) was obtained from Millipore. Rapamycin (R-5000) was obtained from LC laboratories. AICAR (A611700) was obtained from Toronto Research Chemicals. Rhodamine-labeled phalloidin (181-02921) was purchased from Wako Pure Chemical Industries (Osaka, Japan). Rabbit polyclonal antibodies against the following proteins were used: α-catenin (C2081, Sigma-Aldrich, 1:500), and GFP (A6455, Life Technologies, 1:1000). Mouse monoclonal antibodies against the following proteins were used: E-cadherin (610181, BD Transduction Laboratories, 1:500), V5 (R960-25, Invitrogen, 1:500), β-catenin (610154, BD Transduction Laboratories, 1:500), and Flag M2 (F1804, Sigma-Aldrich, 1:1000 for immunoblotting, 1 μg/ml for immunoprecipitation). Rat monoclonal antibody against ZO-1 (sc-33725, 1:500) was purchased from Santa Cruz. Alexa488- and Alexa633-conjugated goat antirabbit IgG (A11034 and A21070, respectively), Alexa488-, Alexa568-, and Alexa633-conjugated goat antimouse IgG (A11029, A11031, and A21052, respectively), Alexa568-conjugated goat antirat IgG (A11077), and Alexa633-conjugated phalloidin (A22284) were purchased from Thermo Fisher Scientific. HRP-conjugated donkey antirabbit IgG (NA934) and sheep antimouse IgG (NA931) were purchased from GE Healthcare.

### Plasmid construction and siRNAs

The expression plasmids encoding YFP-, V5-, and Flag-tagged PLEKHG4B and CFP-tagged ANXA2 were constructed as described previously (Ninomiya *et al.*, 2021). Expression plasmid for mCherry-tagged PLEKHG4B was constructed by inserting the PCR-amplified cDNA into the pmCherry-C1 vector (Clontech, Mountain View, CA). The plasmids encoding deletion mutants of PLEKHG4B were constructed by PCR amplification and subcloning into the Flag-BirA or pEYFP-C1 vector (Clontech), as described previously (Ninomiya *et al.*, 2021). The plasmids encoding K1373A and K1373E mutants of PLEKHG4B were constructed, using a site-directed mutagenesis kit (Agilent Technologies, Santa Clara, CA). $Lyn_{11}$-CFP-FRB, CFP-FRB-MoA, YFP-FKBP-PH(PLCδ), and YFP-FKBP-PI(4)P5K were constructed, as reported (Ueno *et al.*, 2011). pN1-GCaMP6 was a kind gift from Junichi Nakai (Tohoku University; Ohkura *et al.*, 2012). The donor knock-in plasmid was constructed based on the pDonor-tBFP-NLS-Neo (universal) vector containing BbsI/BpiI (Katoh *et al.*, 2017). Briefly, the CMV promoter-tagBFP-NLS sequence of the pDonor-tagBFP-NLS-Neo (universal) plasmid was replaced by PCR-amplified monomeric superfolder (msf)-GFP-PLEKHG4B fragment using NEB Builder HiFi kit (NEB). Double-stranded oligonucleotide targeting the 5′UTR sequence of PLEKHG4B locus (5′-CAGAGGAGGGGCGCTCTCCG-3′) was inserted into the donor knock-in vector and pHiFiCas9-2 × sgRNA (Fujisawa *et al.*, 2021). GFP- and mCherry-PH(PLCδ) were kind gifts from Tomohiko Taguchi and Kojiro Mukai (Tohoku University). The cDNA plasmid for siRNA-resistant (sr)-ANXA2 was constructed by introducing six silent mutations into a target sequence of dog ANXA2 siRNA #1 (5′-GGCGTGAAACGTAAGGGAA-3′, mutated nucleotides are underlined) by using a PrimeSTAR mutagenesis basal kit (Takara). The siRNAs targeting dog E-cadherin, PLEKHG4B, and ANXA2 were purchased from Sigma-Aldrich. The target sequences are as follows: dog E-cadherin #1 (GCA UGA UGU UCA CUA UCA AUU) and #2 (GAC UUU GAC UUG AGC CAG UUU); dog PLEKHG4B #1 (5′-GGU AUG UCA UUG ACC AUU A-3′) and #2 (5′-GAA UAU UCA CAG AAC UCU A-3′); dog ANXA2 #1 (5′-GGA GUG AAG AGG AAA GGA A-3′) and #2 (5′-GGU CUG AAU UCA AGA GAA A-3′). MISSON siRNA Universal Negative Control (Sigma-Aldrich, SIC-001) was used as the negative control siRNA.

### Cell culture and transfection

MDCK and HEK293T cells were cultured in Dulbecco's modified Eagle's medium (DMEM; 044-29765, Wako Pure Chemical) supplemented with 10% fetal calf serum (FCS; Cosmo Bio) at 37°C in 5% $CO_2$. MDCK cells stably expressing V5-PLEKHG4B were established in selection medium containing 2 μg/ml puromycin, as reported (Ninomiya *et al.*, 2021). Plasmid transfection was performed using Lipofectamine LTX and Plus reagent (Thermo Fisher Scientific) for MDCK cells, and jetPEI (Polyplus) for HEK293T cells, according to the manufacture's protocols. Transfection of siRNAs was carried out using Lipofectamine RNAiMAX (Thermo Fisher Scientific). MDCK cells ($1 \times 10^5$ cells/well) were seeded on coverslips in a 12-well culture plate and incubated with the siRNA transfection complex for 48 h. For low $Ca^{2+}$ culture, MDCK cells were incubated in DMEM without glutamine and $Ca^{2+}$ (21068028, Life Technologies) supplemented with 5% $Ca^{2+}$-depleted FBS and 3 μM $Ca^{2+}$ for 3 h. For knockdown-rescue experiments, MDCK cells were plated on

coverslips in 12-well culture plates at an average density of $1.0 \times 10^5$ cells/dish, transfected with plasmids using Lipofectamine LTX and Plus reagent and cultured for 4 h. Then, cells were transfected with siRNAs using Lipofectamine RNAiMAX and cultured for 48 h before microscopic analysis.

### CRISPR/Cas9-mediated knock-in of GFP-PLEKHG4B into the 5′UTR of PLEKHG4B locus

The 5′UTR-targeting knock-in of monomeric superfolder (msf)-GFP-PLEKHG4B in MDCK cells was performed using CRISPR/Cas9 system by homology-independent DNA repair, as described previously (Katoh *et al*., 2017; Fujisawa *et al*., 2021; Ijaz and Ikegami, 2021). The knock-in donor plasmid was constructed by inserting sgRNA sequence of 5′UTR of canine PLEKHG4B gene and msf-GFP-PLEKHG4B sequence into pDonor-tBFP-NLS-Neo (universal; Addgene 80767). MDCK cells ($1 \times 10^5$ cells) seeded onto a 35 $mm^2$ culture dish were transfected with 0.25 µg of knock-in donor plasmid and 1 µg of pHiFiCas9-2 × sgRNA (Addgene 162277), using Lipofectamine LTX reagent (Thermo Fisher Scientifc), and selected in culture medium containing G418 geneticin (750 µg /ml) for 7 d. The plasmids of pDonor-tBFP-NLS-Neo (universal) and pHiFiCas9-2 × sgRNA were kindly gifted by Kazuhisa Nakayama and Yohei Katoh (Kyoto University).

### Immunofluorescence staining and imaging

Cells were cultured on a cover glass, fixed with phosphate-buffered saline (PBS) containing 4% paraformaldehyde (PFA) for 20 min, and then permeabilized with 0.1% Triton X-100 in PBS for 10 min. After washing with PBS, cells were incubated with 2% fetal bovine serum (FBS) to reduce nonspecific antibody binding, before they were probed with the primary antibodies overnight at 4°C. The next day, the cells were washed with PBS, incubated with the secondary antibodies and rhodamine-labeled phalloidin for 60 min, then washed with PBS. Fluorescence images were obtained using an LSM 710 or 980 laser-scanning confocal microscopy (Carl Zeiss, Jena, Germany) equipped with a PL Apo 63× oil objective lens (numerical aperture: 1.4). The images were analyzed in ImageJ software.

### Coimmunoprecipitation assay

For analyzing the binding sites of PLEKHG4B to ANXA2, HEK293T cells were cotransfected with Flag-PLEKHG4B or its deletion mutants and CFP-ANXA2 or its mutants, cultured for 24 h. Cells were lysed with ice-cold lysis buffer (25 mM Tris-HCl, pH 7.4, 1% Triton X-100, 140 mM NaCl, 2.5 mM $MgCl_2$, 1 mM EGTA, 50 mM NaF, 1 mM $Na_3VO_4$, 1 mM PMSF, 10 µg/ml leupeptin, and 2 µg/ml pepstatin A). Cell lysates were clarified by centrifugation at 18,000 xg for 10 min and the supernatants were incubated with anti-Flag antibody and Protein G-Sepharose Fast Flow (GE Healthcare) for 2 h at 4°C. For analyzing the interaction between PLEKHG4B and ANXA2 with or without ionomycin treatment, MDCK cells stably expressing GFP-PLEKHG4B were cultured for 24 h and treated with ionomycin for 15 min. GFP-PLEKHG4B was precipitated with GST-anti-GFP-nanobody prebound to glutathione-Sepharose beads (GE Healthcare). Immunoprecipitates (IPs) were separated by SDS–PAGE and analyzed by immunoblotting.

### Drug treatment

In ionomycin treatment, MDCK cells were transfected with expression plasmids or siRNAs, cultured for 48 h, and then exposed to 2.5 µM ionomycin for 15 min unless otherwise stated. Following incubation, the cells were fixed and analyzed by immunostaining and fluorescence imaging. To examine the effects of drugs, MDCK cells were cultured for 24–48 h to form confluent monolayer and then treated with 10 µM Yoda1, 50 µM Jedi2, 10 µM GsMTx4, or 25 nM BAPTA-AM for 15 min unless otherwise stated. For analyses using a combination of drugs, cells were pretreated with 10 nM BAPTA-AM for 15 min and then exposed to 10 µM ionomycin for 15 min. Following drug treatment, the cells were fixed and subjected to immunofluorescence analysis. To examine the role of AMPK and CaMKK, MDCK cells were transfected with YFP-PLEKHG4B, cultured for 48 h, then treated with 5 µM STO-609, 5 µM Compound C or 25 µM AICAR for 3 h, followed by exposure to 2.5 µM ionomycin for 15 min. In all experiments, dimethyl sulfoxide (DMSO) was used as vehicle control.

### PI(4,5)$P_2$ masking/liberation and synthesis assays

In PI(4,5)$P_2$ masking/liberation assay, MDCK cells were cotransfected with mCherry-PLEKHG4B, CFP-FRB-MoA, and YFP-FKBP-PH(PLCδ). In PI(4,5)$P_2$ synthesis assay, MDCK cells were cotransfected with mCherry-PLEKHG4B, $Lyn_{11}$-CFP-FRB, and YFP-FKBP-PI(4)P5K. Cells were cultured for 24 h, and then treated with 100 nM rapamycin or vehicle for 15 min. Cells were fixed and stained with rhodamine-phalloidin and subjected to immunofluorescence analyses.

### Genomic PCR

To confirm the integration of GFP-PLEKHG4B into the 5′UTR of the PLEKHG4B gene locus in MDCK cells, genomic DNAs were extracted from WT or a mixture of G418-resistant KI cells and subjected to PCR, using KOD FX Neo DNA polymerase (Toyobo) and three sets of primers. Primer sequences used were as follows: Primer 1 (5′-ATC TGC AGG GGG AGG AGG TC-3′), Primer 2 (5′-GCG CTA AAC TGG TCT CTA AGC GAC T3′), Primer 3 (5′-CTC TGG ATA CAG GCA TCA AGA GAT T-3′), and Primer 4 (5′-CGT AAT CTG CTG CTT GCA AAC AAA-3′). Amplified DNA fragments were separated in agarose gel and stained with Midori Green (Nippon Genetics, Japan).

### Semiquantitative RT-PCR

PLEKHG4B knockdown was evaluated by semiquantitative RT-PCR. Total RNA was extracted from the siRNA-transfected MDCK cells with the RNeasy mini kit and QIAshredder (Qiagen), and 1 µg of it was used as a template for first-strand cDNA synthesis using the PrimeScript RT Reagent Kit (Takara), according to the manufacturer's protocol. The cDNA fragments were amplified by PCR using Ex Taq polymerase (Takara), subjected to agarose gel electrophoresis, and imaged by MidoriGreen (Nippon genetics) staining. The expression level of GAPDH was used as an internal control. The primers used were described in our previous paper (Ninomiya *et al*., 2021).

### Statistical analyses

Statistical data are expressed as the mean ± SD of three independent experiments. Statistical analysis was carried out using Prism 9 (GraphPad Software, La Jolla, CA). The *P* values were calculated using a two-tailed paired *t* test or a one-way analysis of variance (ANOVA) followed by Dunnett's test for multiple data set comparisons. In all cases, $P < 0.05$ was considered statistically significant.

## ACKNOWLEDGMENTS

We thank Tomohiko Taguchi and Kojiro Mukai for providing the plasmids for GFP- and mCherry-PH(PLCδ) and their advice, Junichi Nakai (Tohoku University) for providing the plasmid for GCaMP6, and Kazuhisa Nakayama and Yohei Katoh (Kyoto University) for providing the plasmids of pDonor-tBFP-NLS-Neo(universal) and

pHiFiCas9-2 × sgRNA. This work was supported by grants from the Japan Society for the Promotion of Science (JSPS) KAKENHI No. JP21H02471 to K.M., Nos. JP20H03248 and JP22H05618 to K.O., No. JP21H05255 to E.K., and Nos. JP20J12425 and JP22K15095 to K.N., www.jsps.go.jp/j-grantsinaid/, JSPS Fellowship No. JPA16J041330 to K.N., www.jsps.go.jp/j-pd/, Japan Science and Technology Agency (JST) CREST No. JPMJCR1852 to E.K., www.jst.go.jp/EN/, the Japan Agency for Medical Research and Development (AMED) No. JP18gm5810015h0003 to K.O., www.amed.go.jp/en/index.html, the Uehara Memorial Foundation to K.O., and the Japan Foundation for Applied Enzymology to K.O.

## REFERENCES


Arnold TR, Stephenson RE, Miller AL (2017). Rho GTPases and actomyosin: partners in regulating epithelial cell-cell junction structure and function. Exp Cell Res 358, 20–30.

Benink HA, Bement WM (2005). Concentric zones of active RhoA and Cdc42 around single cell wounds. J Cell Biol 168, 429–439.

Bharadwaj A, Bydoun M, Holloway R, Waisman D (2013). Annexin A2 heterotetramer: structure and function. Int J Mol Sci 14, 6259–6305.

Braga V (2018). Signaling by small GTPases at cell-cell junctions: protein interactions building control and networks. Cold Spring Harb Perspect Biol 10, a028746

Bryant DM, Datta A, Rodríguez-Fraticelli AE, PeräCurrency Signnen J, Martín-Belmonte F, Mostov KE (2010). A molecular network for de novo generation of the apical surface and lumen. Nat Cell Biol 12, 1035–1045.

Citi S, Guerrera D, Spadaro D, Shah J (2014). Epithelial junctions and Rho family GTPases: the zonular signalosome. Small GTPases 5, 1–15.

Clapham DE (2007). Calcium signaling. Cell 131, 1047–1058.

Clark AG, Miller AL, Vaughan E, Yu HYE, Penkert R, Bement WM (2009). Integration of single and multicellular wound responses. Curr Biol 19, 1389–1395.

Cook DR, Rossman KL, Der CJ (2014). Rho guanine nucleotide exchange factors: regulators of Rho GTPase activity in development and disease. Oncogene 33, 4021–4035.

Efremov AK, Yao M, Sun Y, Tee YH, Sheetz MP, Bershadsky AD, Martinac B, Yan J (2022). Application of piconewton forces to individual filopodia reveals mechanosensory role of L-type $Ca^{2+}$ channels. Biomaterials 284, 121477.

Evans JH, Murray D, Leslie CC, Falke JJ (2006). Specific translocation of protein kinase Cα to the plasma membrane requires both $Ca^{2+}$ and $PIP_2$ recognition by its C2 domain. Mol Biol Cell 17, 56–66.

Fujisawa S, Qiu H, Nozaki S, Chiba S, Katoh Y, Nakayama K (2021). ARL3 and ARL13B GTPases participate in distinct steps of INPP5E targeting to the ciliary membrane. Biol Open 10, bio058843.

Fukata M, Kaibuchi K (2001). Rho-family GTPases in cadherin-mediated cell-cell adhesion. Nat Rev Mol Cell Biol 2, 887–897.

Garcia MA, Nelson WJ, Chavez N (2018). Cell–cell junctions organize structural and signaling networks. Cold Spring Harb Perspect Biol 10, a029181.

Gerke V, Creutz CE, Moss SE (2005). Annexins: linking $Ca^{2+}$ signalling to membrane dynamics. Nat Rev Mol Cell Biol 6, 449–461.

Hansen MDH, Ehrlich JS, Nelson WJ (2002). Molecular mechanism for orienting membrane and actin dynamics to nascent cell-cell contacts in epithelial cells. J Biol Chem 277, 45371–45376.

Harris T, Tepass U (2010). Adherens junctions: from molecules to morphogenesis. Nat Rev Mol Cell Biol 11, 502–514.

Hashido M, Hayashi K, Hirose K, Iino M (2006). $Ca^{2+}$ lightning conveys cell-cell contact information inside the cells. EMBO Rep 7, 1117–1123.

Hodge RG, Ridley AJ (2016). Regulating Rho GTPases and their regulators. Nat Rev Mol Cell Biol 17, 496–510.

Ijaz F, Ikegami K (2021). Knock-in of labeled proteins into 5'UTR enables highly efficient generation of stable cell lines. Cell Struct Funct 46, 21–35.

Ikebuchi NW, Waisman DM (1990). Calcium-dependent regulation of actin filament bundling by lipocortin-85. J Biol Chem 265, 3392–3400.

Janmey PA, Bucki R, Radhakrishnan R (2018). Regulation of actin assembly by PI(4,5)P2 and other inositol phospholipids: An update on possible mechanisms. Biochem Biophys Res Commun 506, 307–314.

Katoh Y, Michisaka S, Nozaki S, Funabashi T, Hirano T, Takei R, Nakayama K (2017). Practical method for targeted disruption of cilia-related genes by using CRISPR/Cas9-mediated, homology-independent knock-in system. Mol Biol Cell 28, 898–906.

Ko KS, Arora PD, Bhide V, Chen A, McCulloch CAG (2001). Cell-cell adhesion in human fibroblasts requires calcium signaling. J Cell Sci 114, 1155–1167.

Lecuit T, Yap AS (2015). E-cadherin junctions as active mechanical integrators in tissue dynamics. Nat Cell Biol 17, 533–539.

Lemmon MA (2008). Membrane recognition by phospholipid-binding domains. Nat Rev Mol Cell Biol 9, 99–111.

Martin-Belmonte F, Gassama A, Datta A, Yu W, Rescher U, Gerke V, Mostov K (2007). PTEN-mediated apical segregation of phosphoinositides controls epithelial morphogenesis through Cdc42. Cell 128, 383–397.

McCormack J, Welsh NJ, Braga VMM (2013). Cycling around cell-cell adhesion with Rho GTPase regulators. J Cell Sci 126, 379–391.

Mège RM, Ishiyama N (2017). Integration of cadherin adhesion and cytoskeleton at adherens junctions. Cold Spring Harb Perspect Biol 9, a028738.

Murakoshi H, Wang H, Yasuda R (2011). Local, persistent activation of Rho GTPases during plasticity of single dendritic spines. Nature 472, 100–104.

Ninomiya K, Ohta K, Yamashita K, Mizuno K, Ohashi K (2021). PLEKHG4B enables actin cytoskeletal remodeling during epithelial cell-cell junction formation. J Cell Sci, 134, jcs.249078.

Ohashi K, Fujiwara S, Mizuno K (2017). Roles of the cytoskeleton, cell adhesion and rho signaling in mechanosensing and mechanotransduction. J Biochem 161, 245–254.

Ohkura M, Sasaki T, Sadakari J, Gengyo-Ando K, Kagawa-Nagamura Y, Kobayashi C, Ikegaya Y, Nakai J (2012). Genetically encoded green fluorescent $Ca^{2+}$ indicators with improved detectability for neuronal $Ca^{2+}$ signals. PLoS One 7, e51286

Pardo-Pastor C, Rubio-Moscardo F, Vogel-González M, Serra SA, Afthinos A, Mrkonjic S, Destaing O, Abenza JF, Fernández-Fernández JM, Trepat X, *et al.* (2018). Piezo2 channel regulates RhoA and actin cytoskeleton to promote cell mechanobiological responses. Proc Natl Acad Sci USA 115, 1925–1930.

Rajakylä EK, Lehtimäki JI, Acheva A, Schaible N, Lappalainen P, Krishnan R, Tojkander S (2020). Assembly of peripheral actomyosin bundles in epithelial cells is dependent on the CaMKK2/AMPK pathway. Cell Rep 30, 4266–4280.

Rescher U, Ruhe D, Ludwig C, Zobiack N, Gerke V (2004). Annexin 2 is a phosphatidylinositol (4,5)-bisphosphate binding protein recruited to actin assembly sites at cellular membranes. J Cell Sci 117, 3473–3480.

Rossman KL, Der CJ, Sondek J (2005). GEF means go: turning on Rho GTPases with guanine nucleotide-exchange factors. Nat Rev Mol Cell Biol 6, 167–180.

Snyder JT, Rossman KL, Baumeister MA, Pruitt WM, Siderovski DP, Der CJ, Lemmon MA, Sondek J (2001). Quantitative analysis of the effect of phosphoinositide interactions on the function of Dbl family proteins. J Biol Chem 276, 45868–45875.

Takeichi M (2014). Dynamic contacts: rearranging adherens junctions to drive epithelial remodelling. Nat Rev Mol Cell Biol 15, 397–410.

Tojkander S, Ciuba K, Lappalainen P (2018). CaMKK2 regulates mechanosensitive assembly of contractile actin stress fibers. Cell Rep 24, 11–19.

Tsai FC, Kuo GH, Chang SW, Tsai PJ (2015). $Ca^{2+}$ signaling in cytoskeletal reorganization, cell migration, and cancer metastasis. Biomed Res Int 2015, 409245

Ueno T, Falkenburger BH, Pohlmeyer C, Inoue T (2011). Triggering actin comets versus membrane ruffles: distinctive effects of phosphoinositides on actin reorganization. Sci Signal 4, ra87.

Varadarajan S, Chumki SA, Stephenson RE, Misterovich ER, Wu JL, Dudley CE, Erofeev IS, Goryachev AB, Miller AL (2022). Mechanosensitive calcium flashes promote sustained RhoA activation during tight junction remodeling. J Cell Biol 221, e202105107.

Yamada A, Irie K, Hirota T, Ooshio T, Fukuhara,A, Takai Y (2005). Involvement of the annexin II-S100A10 complex in the formation of E-cadherin-based adherens junctions in Madin-Darby canine kidney cells. J Biol Chem 280, 6016–6027.

Yang W, Wu P, Ma J, Liao M, Xu L, Yi L (2020). TRPV4 activates the Cdc42/N-wasp pathway to promote glioblastoma invasion by altering cellular protrusions. Sci Rep 10, 14151.

Yao M, Tijore A, Cheng D, Li JV, Hariharan A, Martinac B, Tran Van Nhieu G, Cox CD, Sheetz M (2022). Force- and cell state-dependent recruitment of Piezo1 drives focal adhesion dynamics and calcium entry. Sci Adv 8, eabo1461.

Yeung T, Terebiznik M, Yu L, Silvius J, Abidi WM, Philips M, Levine T, Kapus A, Grinstein S (2006). Receptor activation alters inner surface potential during phagocytosis. Science 313, 347–351.